SIAM J. APPL. MATH.
Vol. 66, No. 3, pp. 758–786

DYNAMICS OF ROTATING BOSE–EINSTEIN CONDENSATES AND ITS EFFICIENT AND ACCURATE NUMERICAL COMPUTATION *

WEIZHU BAO†, QIANG DU‡, AND YANZHI ZHANG§

Abstract. In this paper, we study the dynamics of rotating Bose–Einstein condensates (BEC) based on the Gross–Pitaevskii equation (GPE) with an angular momentum rotation term and present an efficient and accurate algorithm for numerical simulations. We examine the conservation of the angular momentum expectation and the condensate width and analyze the dynamics of a stationary state with a shift in its center. By formulating the equation in either the two-dimensional polar coordinate system or the three-dimensional cylindrical coordinate system, the angular momentum rotation term becomes a term with constant coefficients. This allows us to develop an efficient time-splitting method which is time reversible, unconditionally stable, efficient, and accurate for the problem. Moreover, it conserves the position density. We also apply the numerical method to study issues such as the stability of central vortex states and the quantized vortex lattice dynamics in rotating BEC.

Key words. rotating Bose–Einstein condensation, Gross–Pitaevskii equation, angular momentum rotation, time-splitting, ground state, central vortex state, energy, condensate width, angular momentum expectation

AMS subject classifications. 35Q55, 65T99, 65Z05, 65N12, 65N35, 81-08

DOI. 10.1137/050629392

1. Introduction.

Since its realization in dilute bosonic atomic gases [3, 20, 21], Bose–Einstein condensation of alkali atoms and hydrogen has been produced and studied extensively in the laboratory [45] and has permitted an intriguing glimpse into the macroscopic quantum world. In view of potential applications [26, 43, 44], the study of quantized vortices, which are well-known signatures of superfluidity, is one of the key issues. Different research groups have obtained quantized vortices in Bose–Einstein condensates (BEC) experimentally, e.g., the JILA group [39], the ENS group [36, 37], and the MIT group [45]. Currently, there are at least two typical ways to generate quantized vortices from the ground state of BEC: (i) impose a laser beam rotating with an angular velocity on the magnetic trap holding the atoms to create an harmonic anisotropic potential [17, 33, 1, 13]; (ii) add to the stationary magnetic trap a narrow, moving Gaussian potential, representing a far-blue detuned laser [29, 7]. The recent experimental and theoretical advances in the exploration of quantized vortices in BEC have spurred great excitement in the atomic physics community and renewed interest in studying superfluidity.

The properties of BEC in a rotational frame at temperature T much smaller than the critical condensation temperature T_c are well described by the macroscopic

*Received by the editors April 18, 2005; accepted for publication (in revised form) September 12, 2005; published electronically February 3, 2006. This work was partially done while the first two authors were visiting the Institute for Mathematical Sciences, National University of Singapore, in 2005. The visit was supported by the Institute.

http://www.siam.org/journals/siap/66-3/62939.html

†Department of Mathematics, National University of Singapore, 117543 Singapore (bao@cz3.nus.edu.sg, http://www.cz3.nus.edu.sg/∼bao/). The research of this author was supported by the National University of Singapore grant R-151-000-035-112.

‡Department of Mathematics, Penn State University, University Park, PA 16802 (qdu@math.psu.edu, http://www.math.psu.edu/qdu). The research of this author was supported by NSF DMS 0409297 and ITR 0205232.

§Department of Mathematics, National University of Singapore, 117543 Singapore (zhyanzhi@cz3.nus.edu.sg).

wave function $\psi(\mathbf{x},t)$, whose evolution is governed by a self-consistent, mean field nonlinear Schrödinger equation (NLSE) in a rotational frame, also known as the Gross–Pitaevskii equation (GPE) with an angular momentum rotation term [26, 17, 24, 25, 15]:

(1.1)
$$i\hbar\partial_t\psi(\mathbf{x},t) = \left(-\frac{\hbar^2}{2m}\nabla^2 + V(\mathbf{x}) + NU_0|\psi|^2 - \Omega L_z\right)\psi(\mathbf{x},t), \quad \mathbf{x}\in\mathbb{R}^3, \quad t\geq 0,$$

where $\mathbf{x} = (x,y,z)^T$ is the Cartesian coordinate vector, m is the atomic mass, $\hbar$ is the Planck constant, N is the number of atoms in the condensate, Ω is the angular velocity of the rotating laser beam, and $V(\mathbf{x})$ is an external trapping potential. When an harmonic trap potential is considered, $V(\mathbf{x}) = \frac{m}{2}\left(\omega_x^2x^2+\omega_y^2y^2+\omega_z^2z^2\right)$ with ω_x, ω_y, and ω_z being the trap frequencies in the x-, y-, and z-direction, respectively. $U_0 = \frac{4\pi\hbar^2a_s}{m}$ describes the interaction between atoms in the condensate with a_s (positive for repulsive interaction and negative for attractive interaction) the s-wave scattering length, and $L_z = xp_y - yp_x = -i\hbar\left(x\partial_y - y\partial_x\right)$ is the z-component of the angular momentum $\mathbf{L} = \mathbf{x}\times\mathbf{P}$ with the momentum operator $\mathbf{P} = -i\hbar\nabla = (p_x,p_y,p_z)^T$. It is convenient to normalize the wave function by requiring that

(1.2)
$$\|\psi(\cdot,t)\|^2 := \int_{\mathbb{R}^3}|\psi(\mathbf{x},t)|^2d\mathbf{x} = 1.$$

Under such a normalization, we introduce the dimensionless variables as follows: $t\to t/\omega_m$ with $\omega_m = \min\{\omega_x,\omega_y,\omega_z\}$, $\Omega\to\omega_m\Omega$, $\mathbf{x}\to a_0\mathbf{x}$ with $a_0 = \sqrt{\frac{\hbar}{m\omega_m}}$, and $\psi\to\psi/a_0^{3/2}$. We also let

$$\gamma_x = \frac{\omega_x}{\omega_m}, \quad \gamma_y = \frac{\omega_y}{\omega_m}, \quad \gamma_z = \frac{\omega_z}{\omega_m}, \quad \beta = \frac{U_0N}{a_0^3\hbar\omega_m} = \frac{4\pi a_sN}{a_0}.$$

The dimensionless angular momentum rotational term then becomes

(1.3)
$$L_z = -i(x\partial_y - y\partial_x) = i(y\partial_x - x\partial_y) = -i\partial_\theta$$

with (r,θ) being the polar coordinates in two dimensions (2D) and (r,θ,z) the cylindrical coordinates in three dimensions (3D). In the disk-shaped condensation, i.e., $\omega_y\approx\omega_x$ and $\omega_z\gg\omega_x$ ($\Leftrightarrow\gamma_x = 1$, $\gamma_y\approx 1$, and $\gamma_z\gg 1$ with choosing $\omega_m = \omega_x$), the three-dimensional GPE can be reduced to a two-dimensional GPE [13]. Thus, here we consider the dimensionless GPE with a rotational term in the d-dimensions ($d = 2,3$) [13]:

(1.4)
$$i\partial_t\psi(\mathbf{x},t) = -\frac{1}{2}\nabla^2\psi + V_d(\mathbf{x})\psi + \beta_d|\psi|^2\psi - \Omega L_z\psi, \quad \mathbf{x}\in\mathbb{R}^d, \quad t>0,$$

(1.5)
$$\psi(\mathbf{x},0) = \psi_0(\mathbf{x}), \quad \mathbf{x}\in\mathbb{R}^d, \quad \text{with} \quad \|\psi_0\|^2 := \int_{\mathbb{R}^d}|\psi_0(\mathbf{x})|^2d\mathbf{x} = 1,$$

where

(1.6)
$$\beta_d = \begin{cases}\beta\sqrt{\gamma_z/2\pi}, & \\ \beta, & \end{cases} \qquad V_d(\mathbf{x}) = \begin{cases}(\gamma_x^2x^2+\gamma_y^2y^2)/2, & d=2,\\ (\gamma_x^2x^2+\gamma_y^2y^2+\gamma_z^2z^2)/2, & d=3,\end{cases}$$

with $\gamma_x > 0$, $\gamma_y > 0$, and $\gamma_z > 0$ being constants. Two important invariants of (1.4) are the *normalization of the wave function*

$$N(\psi) = \int_{\mathbb{R}^d} |\psi(\mathbf{x},t)|^2 d\mathbf{x} \equiv \int_{\mathbb{R}^d} |\psi(\mathbf{x},0)|^2 d\mathbf{x} = N(\psi_0) = 1, \qquad t \geq 0, \tag{1.7}$$

and the *energy*

$$\begin{aligned} E_{\beta,\Omega}(\psi) &= \int_{\mathbb{R}^d} \left[\frac{1}{2}|\nabla\psi|^2 + V_d(\mathbf{x})|\psi|^2 + \frac{\beta_d}{2}|\psi|^4 - \Omega \mathrm{Re}(\psi^* L_z \psi) \right] d\mathbf{x} \\ &\equiv E_{\beta,\Omega}(\psi_0), \qquad t \geq 0, \end{aligned} \tag{1.8}$$

where f^* and $\mathrm{Re}f$ denote the conjugate and the real part of the function f, respectively.

In order to study effectively the dynamics of BEC, especially in the strong repulsive interaction regime, i.e., $\beta_d \gg 1$ in (1.4), an efficient and accurate numerical method is one of the key issues. For nonrotating BEC, i.e., $\Omega = 0$ in (1.4), many numerical methods were proposed in the literature. For example, Bao, Jaksch, and Markowich [7], Bao and Jaksch [6], and Bao and Zhang [14] proposed a fourth-order time-splitting sine or Fourier pseudospectral (TSSP) method, and Bao and Shen [11] presented a fourth-order time-splitting Laguerre–Hermite (TSLH) pseudospectral method for the GPE when the external trapping potential is radially or cylindrically symmetric in 2D or 3D. The key ideas for the numerical methods in [7, 4, 6, 14, 11, 9, 10] are based on (i) a time-splitting technique being applied to decouple the nonlinearity in the GPE [7, 6, 9, 10]; (ii) proper spectral basis functions being chosen for a linear Schrödinger equation with a potential such that the ODE system in phase space is diagonalized and thus can be integrated exactly [14, 11]. These methods are explicit, unconditionally stable, and of spectral accuracy in space and fourth-order accuracy in time. Thus they are very efficient and accurate for computing the dynamics of nonrotating BEC in 3D [8] and for multicomponent [4]. Some other numerical methods for nonrotating BEC include the finite difference method [18, 41, 40], the particle-inspired scheme [19, 40], and the Runge–Kutta pseudospectral method [16, 40]. Due to the appearance of the angular momentum rotation term in the GPE (1.4), the TSSP and TSLH methods proposed in [7, 14, 11] can no longer be used for rotating BEC. Currently, the numerical methods proposed in the literature for studying the dynamics of rotating BEC remain limited [1, 22, 33], and they usually are low-order methods. Thus it is of great interest to develop an efficient, accurate, and unconditionally stable numerical method for the GPE (1.4) with an angular momentum rotation term. Such a numerical method is proposed here and is applied to the study of the dynamics of the rotating BEC. The key features of our numerical method are based on (i) the application of a time-splitting technique for decoupling the nonlinearity in the GPE; (ii) the adoption of polar coordinates or cylindrical coordinates so as to make the coefficient of the angular momentum rotation term constant; (iii) the utilization of Fourier pseudospectral discretization in the transverse direction and a second- or fourth-order finite difference or finite element discretization in the radial direction. Our extensive numerical results demonstrate that the method is very efficient and accurate.

The paper is organized as follows. In section 2, the conservation of the angular momentum expectation and the dynamics of condensate widths are first established. We then analyze the stationary state with a shift in its center and provide some study on the decrease of the total density in the presence of dissipation. In section 3, a

numerical method is presented for the efficient and accurate simulation of GPE (1.4) in 2D and 3D. It is then applied to study the vortex state and the dynamics of rotating BEC in section 4. Finally, some conclusions are drawn in section 5.

2. Dynamics of rotating BEC. In this section, we provide some analytical results on the conservation of the angular momentum expectation in a symmetric trap, i.e., $\gamma_x = \gamma_y$ in (1.6), derive a second-order ODE for time evolution of the condensate width, and present some dynamic laws of a stationary state with a shifted center in rotating BEC.

2.1. Conservation of angular momentum expectation. As a measure of the vortex flux, we define the angular momentum expectation:

$$\langle L_z\rangle(t) := \int_{\mathbb{R}^d} \psi^*(\mathbf{x},t) L_z \psi(\mathbf{x},t)\, d\mathbf{x} = i\int_{\mathbb{R}^d} \psi^*(\mathbf{x},t)(y\partial_x - x\partial_y)\psi(\mathbf{x},t) d\mathbf{x} \tag{2.1}$$

for any $t \geq 0$. For the dynamics of angular momentum expectation in rotating BEC, we have the following lemma.

LEMMA 2.1. *Suppose $\psi(\mathbf{x},t)$ is the solution of the problem* (1.4)–(1.5)*; then we have*

$$\frac{d\langle L_z\rangle(t)}{dt} = \left(\gamma_x^2 - \gamma_y^2\right)\delta_{xy}(t), \quad \textit{where } \delta_{xy}(t) = \int_{\mathbb{R}^d} xy|\psi(\mathbf{x},t)|^2 d\mathbf{x}, \quad t \geq 0. \tag{2.2}$$

Consequently, the angular momentum expectation and energy for the nonrotating part are conserved; that is, for any given initial data $\psi_0(\mathbf{x})$ in (1.5)*,*

$$\langle L_z\rangle(t) \equiv \langle L_z\rangle(0), \quad E_{\beta,0}(\psi) \equiv E_{\beta,0}(\psi_0), \quad t \geq 0, \tag{2.3}$$

at least for radially symmetric trap in 2D or cylindrically symmetric trap in 3D, i.e., $\gamma_x = \gamma_y$.

Proof. Differentiating (2.1) with respect to t, noticing (1.4), integrating by parts, and taking into account that ψ decreases to 0 exponentially when $|\mathbf{x}| \to \infty$, we have

$$\begin{aligned}
&\frac{d\langle L_z\rangle(t)}{dt} \\
&= i\int_{\mathbb{R}^d} \left[\psi_t^*(y\partial_x - x\partial_y)\psi + \psi^*(y\partial_x - x\partial_y)\psi_t\right] d\mathbf{x} \\
&= \int_{\mathbb{R}^d} \left[(-i\psi_t^*)\,(x\partial_y - y\partial_x)\psi + (i\psi_t)\,(x\partial_y - y\partial_x)\psi^*\right] d\mathbf{x} \\
&= \int_{\mathbb{R}^d} \Bigg[\left(-\frac{1}{2}\nabla^2\psi^* + V_d(\mathbf{x})\psi^* + \beta_d|\psi|^2\psi^* - i\Omega(x\partial_y - y\partial_x)\psi^*\right)(x\partial_y - y\partial_x)\psi \\
&\qquad + \left(-\frac{1}{2}\nabla^2\psi + V_d(\mathbf{x})\psi + \beta_d|\psi|^2\psi + i\Omega(x\partial_y - y\partial_x)\psi\right)(x\partial_y - y\partial_x)\psi^*\Bigg] d\mathbf{x} \\
&= \int_{\mathbb{R}^d} \Bigg[-\frac{1}{2}\left[\nabla^2\psi^*(x\partial_y - y\partial_x)\psi + \nabla^2\psi(x\partial_y - y\partial_x)\psi^*\right] \\
&\qquad + \left(V_d(\mathbf{x}) + \beta_d|\psi|^2\right)\left[\psi^*(x\partial_y - y\partial_x)\psi + \psi(x\partial_y - y\partial_x)\psi^*\right]\Bigg] d\mathbf{x} \\
&= -\int_{\mathbb{R}^d} |\psi|^2(x\partial_y - y\partial_x)V_d(\mathbf{x}) d\mathbf{x} = \left(\gamma_x^2 - \gamma_y^2\right)\int_{\mathbb{R}^d} xy|\psi|^2 d\mathbf{x}, \quad t \geq 0,
\end{aligned} \tag{2.4}$$

which gives (2.2). As for the conservation properties, since $\gamma_x = \gamma_y$, (2.2) reduces to the first-order ODE:

$$\frac{d\langle L_z\rangle(t)}{dt} = 0, \qquad t \geq 0. \tag{2.5}$$

We thus get the conservation of $\langle L_z\rangle$ immediately.

Noticing $E_{\beta,\Omega}(\psi) = E_{\beta,0}(\psi) - \Omega \mathrm{Re}\langle L_z\rangle$ and $\mathrm{Re}\langle L_z\rangle = \langle L_z\rangle$, we get (2.3) from (2.5) and (1.8). ∎

2.2. Dynamics of condensate widths. Another quantity characterizing the dynamics of rotating BEC is the condensate width defined as

$$\sigma_\alpha(t) = \sqrt{\delta_\alpha(t)}, \quad \text{where } \delta_\alpha(t) = \langle \alpha^2\rangle(t) = \int_{\mathbb{R}^d} \alpha^2 |\psi(\mathbf{x},t)|^2 d\mathbf{x} \tag{2.6}$$

for $t \geq 0$ and α being x, y, or z. For the dynamics of condensate widths, we have the following lemmas.

LEMMA 2.2. *Suppose $\psi(\mathbf{x},t)$ is the solution of problem (1.4)–(1.5); then we have*

$$\begin{aligned}\frac{d^2\delta_\alpha(t)}{dt^2} = \int_{\mathbb{R}^d} \Big[&(\partial_y \alpha - \partial_x \alpha)\left(4i\Omega\psi^*(x\partial_y + y\partial_x)\psi + 2\Omega^2(x^2-y^2)|\psi|^2\right) \\ &+ 2|\partial_\alpha \psi|^2 + \beta_d |\psi|^4 - 2\alpha|\psi|^2 \partial_\alpha(V_d(\mathbf{x}))\Big] d\mathbf{x}, \qquad t \geq 0,\end{aligned} \tag{2.7}$$

$$\delta_\alpha(0) = \delta_\alpha^{(0)} = \int_{\mathbb{R}^d} \alpha^2 |\psi_0(\mathbf{x})|^2 d\mathbf{x}, \qquad \alpha = x, y, z, \tag{2.8}$$

$$\dot{\delta}_\alpha(0) = \delta_\alpha^{(1)} = 2\int_{\mathbb{R}^d} \alpha \left[-\Omega|\psi_0|^2 (x\partial_y - y\partial_x)\alpha + \mathrm{Im}\left(\psi_0^* \partial_\alpha \psi_0\right)\right] d\mathbf{x}, \tag{2.9}$$

where $\mathrm{Im}(f)$ *denotes the imaginary part of* f.

Proof. Differentiating (2.6) with respect to t, applying (1.4), and integrating by parts, we obtain

$$\begin{aligned}\frac{d\delta_\alpha(t)}{dt} &= \frac{d}{dt}\int_{\mathbb{R}^d} \alpha^2 |\psi(\mathbf{x},t)|^2 d\mathbf{x} = \int_{\mathbb{R}^d} \alpha^2 \left(\psi \partial_t \psi^* + \psi^* \partial_t \psi\right) d\mathbf{x} \\ &= \int_{\mathbb{R}^d} \left[\frac{i}{2}\alpha^2 \left(\psi^* \nabla^2 \psi - \psi \nabla^2 \psi^*\right) + \Omega \alpha^2 \left(x\partial_y - y\partial_x\right)|\psi|^2\right] d\mathbf{x} \\ &= \int_{\mathbb{R}^d} \left[i\alpha\left(\psi \partial_\alpha \psi^* - \psi^* \partial_\alpha \psi\right) - 2\Omega\alpha|\psi|^2 \left(x\partial_y - y\partial_x\right)\alpha\right] d\mathbf{x}.\end{aligned} \tag{2.10}$$

Differentiating the above equation again, applying (1.4), and integrating by parts, we get

$$\begin{aligned}&\frac{d^2\delta_\alpha(t)}{dt^2} \\ &= \int_{\mathbb{R}^d} \Big[i\alpha\left(\partial_t\psi \partial_\alpha \psi^* + \psi \partial_{\alpha t}\psi^* - \partial_t \psi^* \partial_\alpha \psi - \psi^* \partial_{\alpha t}\psi\right) \\ &\qquad - 2\Omega\alpha\left(\psi\partial_t\psi^* + \psi^*\partial_t\psi\right)\left(x\partial_y - y\partial_x\right)\alpha\Big] d\mathbf{x} \\ &= \int_{\mathbb{R}^d} \Big[2i\alpha\left(\partial_t\psi\partial_\alpha\psi^* - \partial_t\psi^*\partial_\alpha\psi\right) + i\left(\psi^*\partial_t\psi - \psi\partial_t\psi^*\right) \\ &\qquad - 2\Omega\alpha(x\partial_y - y\partial_x)\alpha\left(\frac{i}{2}\left(\psi^*\nabla^2\psi - \psi\nabla^2\psi^*\right) + \Omega(x\partial_y - y\partial_x)|\psi|^2\right)\Big] d\mathbf{x},\end{aligned} \tag{2.11}$$

$$
\begin{aligned}
&\frac{d^2\delta_\alpha(t)}{dt^2}\\
&= \int_{\mathbb{R}^d}\Bigg[-\alpha\left(\partial_\alpha\psi^*\nabla^2\psi + \partial_\alpha\psi\nabla^2\psi^*\right) + 2\alpha\left(V_d(\mathbf{x}) + \beta_d|\psi|^2\right)\left(\psi\partial_\alpha\psi^* + \psi^*\partial_\alpha\psi\right)\\
&\qquad -2i\Omega\alpha\left[\partial_\alpha\psi\left(x\partial_y - y\partial_x\right)\psi^* - \partial_\alpha\psi^*\left(x\partial_y - y\partial_x\right)\psi\right] - \frac{1}{2}\left(\psi^*\nabla^2\psi + \psi\nabla^2\psi^*\right)\\
&\qquad +2\left(V_d(\mathbf{x})|\psi|^2 + \beta_d|\psi|^4\right) - i\Omega\left[\psi\left(x\partial_y - y\partial_x\right)\psi^* - \psi^*\left(x\partial_y - y\partial_x\right)\psi\right]\\
&\qquad -2i\Omega\psi^*\left[\partial_x\alpha\left(\alpha\partial_y + y\partial_\alpha\right)\psi - \partial_y\alpha\left(\alpha\partial_x + x\partial_\alpha\right)\psi\right]\\
&\qquad +2\Omega^2|\psi|^2\left[\left(y^2 - \alpha x\right)\partial_x\alpha + \left(x^2 - \alpha y\right)\partial_y\alpha\right]\Bigg] d\mathbf{x}\\
&= \int_{\mathbb{R}^d}\Big[-4i\Omega\psi^*\left[\partial_x\alpha\left(\alpha\partial_y + y\partial_\alpha\right)\psi - \partial_y\alpha\left(\alpha\partial_x + x\partial_\alpha\right)\psi\right] + 2|\partial_\alpha\psi|^2 + \beta_d|\psi|^4\\
&\qquad +2\Omega^2|\psi|^2\left[\left(y^2 - \alpha x\right)\partial_x\alpha + \left(x^2 - \alpha y\right)\partial_y\alpha\right] - 2\alpha|\psi|^2\partial_\alpha\left(V_d(\mathbf{x})\right)\Big] d\mathbf{x}\\
&= \int_{\mathbb{R}^d}\Big[\left(\partial_y\alpha - \partial_x\alpha\right)\left[4i\Omega\psi^*(x\partial_y + y\partial_x)\psi + 2\Omega^2\left(x^2 - y^2\right)|\psi|^2\right]\\
&\qquad +2|\partial_\alpha\psi|^2 + \beta_d|\psi|^4 - 2\alpha|\psi|^2\partial_\alpha\left(V_d(\mathbf{x})\right)\Big] d\mathbf{x}. \qquad (2.12)
\end{aligned}
$$

Furthermore, noticing (1.5), (2.6), and (2.10) with $t = 0$, we get (2.8) and (2.9) immediately. □

LEMMA 2.3. (i) *In 2D with a radial symmetric trap, i.e., $d = 2$ and $\gamma_x = \gamma_y := \gamma_r$ in* (1.4)*, for any initial data $\psi_0 = \psi_0(x, y)$, we have, for any $t \geq 0$,*

$$
\delta_r(t) = \frac{E_{\beta,\Omega}(\psi_0) + \Omega\langle L_z\rangle(0)}{\gamma_r^2}\left[1 - \cos(2\gamma_r t)\right] + \delta_r^{(0)}\cos(2\gamma_r t) + \frac{\delta_r^{(1)}}{2\gamma_r}\sin(2\gamma_r t), \qquad (2.13)
$$

where $\delta_r(t) = \delta_x(t) + \delta_y(t)$, $\delta_r^{(0)} := \delta_x(0) + \delta_y(0)$, and $\delta_r^{(1)} := \dot\delta_x(0) + \dot\delta_y(0)$. Furthermore, when the initial condition $\psi_0(x, y)$ in (1.5) *satisfies*

$$
\psi_0(x, y) = f(r)e^{im\theta} \quad \text{with} \quad m \in \mathbb{Z} \quad \text{and} \quad f(0) = 0 \quad \text{when} \quad m \neq 0, \qquad (2.14)
$$

we have, for any $t \geq 0$,

$$
\begin{aligned}
\delta_x(t) = \delta_y(t) &= \frac{1}{2}\delta_r(t)\\
&= \frac{E_{\beta,\Omega}(\psi_0) + m\Omega}{2\gamma_x^2}\left[1 - \cos(2\gamma_x t)\right] + \delta_x^{(0)}\cos(2\gamma_x t) + \frac{\delta_x^{(1)}}{2\gamma_x}\sin(2\gamma_x t). \qquad (2.15)
\end{aligned}
$$

This and (2.6) *imply that*

$$
\sigma_x = \sigma_y = \sqrt{\frac{E_{\beta,\Omega}(\psi_0) + m\Omega}{2\gamma_x^2}\left[1 - \cos(2\gamma_x t)\right] + \delta_x^{(0)}\cos(2\gamma_x t) + \frac{\delta_x^{(1)}}{2\gamma_x}\sin(2\gamma_x t)}. \qquad (2.16)
$$

Thus in this case, the condensate widths $\sigma_x(t)$ and $\sigma_y(t)$ are periodic functions with frequency doubling the trapping frequency.

(ii) *For all other cases, we have, for any* $t \geq 0$,

$$\delta_\alpha(t) = \frac{E_{\beta,\Omega}(\psi_0)}{\gamma_\alpha^2} + \left(\delta_\alpha^{(0)} - \frac{E_{\beta,\Omega}(\psi_0)}{\gamma_\alpha^2}\right)\cos(2\gamma_\alpha t) + \frac{\delta_\alpha^{(1)}}{2\gamma_\alpha}\sin(2\gamma_\alpha t) + f_\alpha(t), \tag{2.17}$$

where $f_\alpha(t)$ *is the solution of the following second-order ODE:*

$$\frac{d^2 f_\alpha(t)}{dt^2} + 4\gamma_\alpha^2\, f_\alpha(t) = F_\alpha(t), \qquad f_\alpha(0) = \frac{df_\alpha(0)}{dt} = 0, \tag{2.18}$$

with

$$\begin{aligned} F_\alpha(t) = \int_{\mathbb{R}^d} \Big[& 2|\partial_\alpha\psi|^2 - 2|\nabla\psi|^2 - \beta_d|\psi|^4 + \left(2\gamma_\alpha^2\alpha^2 - 4V_d(\mathbf{x})\right)|\psi|^2 + 4\Omega\psi^* L_z\psi \\ & + (\partial_y\alpha - \partial_x\alpha)\left(4i\Omega\psi^*\left(x\partial_y + y\partial_x\right)\psi + 2\Omega^2(x^2-y^2)|\psi|^2\right)\Big] d\mathbf{x}. \end{aligned}$$

Proof. From (2.7) with $d = 2$, we have

$$\begin{aligned} & \frac{d^2\delta_x(t)}{dt^2} + 2\gamma_x^2\delta_x(t) \\ & = \int_{\mathbb{R}^2}\left[2|\partial_x\psi|^2 + \beta_2|\psi|^4 - 4i\Omega\psi^*\left(x\partial_y + y\partial_x\right)\psi - 2\Omega^2\left(x^2-y^2\right)|\psi|^2\right] d\mathbf{x}, \end{aligned} \tag{2.19}$$

$$\begin{aligned} & \frac{d^2\delta_y(t)}{dt^2} + 2\gamma_y^2\delta_y(t) \\ & = \int_{\mathbb{R}^2}\left[2|\partial_y\psi|^2 + \beta_2|\psi|^4 + 4i\Omega\psi^*\left(x\partial_y + y\partial_x\right)\psi + 2\Omega^2\left(x^2-y^2\right)|\psi|^2\right] d\mathbf{x}. \end{aligned} \tag{2.20}$$

For case (i) with $\gamma_x = \gamma_y := \gamma_r$ in (1.4), summing up (2.19) and (2.20) together and applying (1.8) and (2.3), we have the following ODE for $\delta_r(t)$:

$$\begin{aligned} \frac{d^2\delta_r(t)}{dt^2} &= -2\gamma_r^2\delta_r(t) + \int_{\mathbb{R}^2}\left[2|\nabla\psi|^2 + 2\beta_2|\psi|^4\right] d\mathbf{x} \\ &= -2\gamma_r^2\delta_r(t) - 4\int_{\mathbb{R}^2}\left[V_2(\mathbf{x})|\psi|^2 - \Omega\psi^* L_z\psi\right] d\mathbf{x} \\ &\quad + 4\int_{\mathbb{R}^2}\left[\frac{1}{2}|\nabla\psi|^2 + V_2(\mathbf{x})|\psi|^2 + \frac{\beta_2}{2}|\psi|^4 - \Omega\psi^* L_z\psi\right] d\mathbf{x} \\ &= -2\gamma_r^2\delta_r(t) - 2\gamma_r^2\delta r(t) + 4\Omega\langle L_z\rangle(t) + 4E_{\beta,\Omega}(\psi(\cdot,t)) \\ &= -4\gamma_r^2\delta_r(t) + 4E_{\beta,\Omega}(\psi_0) + 4\Omega\langle L_z\rangle(0), \qquad t \geq 0, \end{aligned} \tag{2.21}$$

$$\delta_r(0) = \delta_r^{(0)}, \qquad \dot{\delta}_r(0) = \delta_r^{(1)}. \tag{2.22}$$

Thus, (2.13) is the unique solution of the second-order ODE (2.21) with the initial data (2.22). Furthermore, when the initial data $\psi_0(\mathbf{x})$ in (1.5) satisfies (2.14), due to symmetry, the solution $\psi(\mathbf{x},t)$ of (1.4)–(1.5) satisfies

$$\psi(x,y,t) = g(r,t)e^{im\theta} \quad \text{with} \quad g(r,0) = f(r). \tag{2.23}$$

This implies

$$\begin{aligned}\delta_x(t) &= \int_{\mathbb{R}^2} x^2|\psi(x,y,t)|^2\,d\mathbf{x} = \int_0^\infty\int_0^{2\pi} r^2\cos^2\theta|g(r,t)|^2 r\,d\theta dr\\ &= \pi\int_0^\infty r^2|g(r,t)|^2 r\,dr = \int_0^\infty\int_0^{2\pi} r^2\sin^2\theta|g(r,t)|^2 r\,d\theta dr\\ &= \int_{\mathbb{R}^2} y^2|\psi(x,y,t)|^2\,d\mathbf{x} = \delta_y(t), \qquad t\ge 0. \end{aligned} \tag{2.24}$$

Since $\gamma_x = \gamma_y$, by Lemma 2.1, we know in this case that

$$\begin{aligned}\langle L_z\rangle(t) &= \langle L_z\rangle(0) = -i\int_{\mathbb{R}^2}\psi_0^*(x,y)\partial_\theta\psi_0(x,y)\,d\mathbf{x}\\ &= 2\pi m\int_0^\infty |f(r)|^2 r\,dr = m\|\psi_0\|^2 = m.\end{aligned} \tag{2.25}$$

Thus, (2.15) is a combination of (2.13), (2.24), and (2.25).

(ii) From (2.7) and noticing the energy conservation (1.8), we have

$$\begin{aligned}\frac{d^2\delta_\alpha(t)}{dt^2} &= \int_{\mathbb{R}^d}\Big[(\partial_y\alpha-\partial_x\alpha)\left[4i\Omega\psi^*(x\partial_y+y\partial_x)\psi+2\Omega^2\left(x^2-y^2\right)|\psi|^2\right]\\ &\qquad +2|\partial_\alpha\psi|^2+\beta_d|\psi|^4-2\gamma_\alpha^2\alpha^2|\psi|^2\Big]\,d\mathbf{x}\\ &= -4\gamma_\alpha^2\delta_\alpha(t)+4\int_{\mathbb{R}^2}\left[\frac{1}{2}|\nabla\psi|^2+V_d(\mathbf{x})|\psi|^2+\frac{\beta_d}{2}|\psi|^4-\Omega\psi^*L_z\psi\right]d\mathbf{x}\\ &\quad+\int_{\mathbb{R}^d}\Big[2|\partial_\alpha\psi|^2-2|\nabla\psi|^2-\beta_d|\psi|^4+\left(2\gamma_\alpha^2\alpha^2-4V_d(\mathbf{x})\right)|\psi|^2+4\Omega\psi^*L_z\psi\\ &\qquad+(\partial_y\alpha-\partial_x\alpha)\left(4i\Omega\psi^*\left(x\partial_y+y\partial_x\right)\psi+2\Omega^2(x^2-y^2)|\psi|^2\right)\Big]d\mathbf{x}\\ &= -4\gamma_\alpha^2\delta_\alpha(t)+4E_{\beta,\Omega}(\psi(\cdot,t))+F_\alpha(t)\\ &= -4\gamma_\alpha^2\delta_\alpha(t)+4E_{\beta,\Omega}(\psi_0)+F_\alpha(t), \qquad t\ge 0.\end{aligned} \tag{2.26}$$

Thus (2.17) is the unique solution of the second-order ODE (2.26) with the initial data (2.8), (2.9). ∎

2.3. Dynamics of a stationary state with its center shifted. Let $\phi_e(\mathbf{x})$ be a stationary state of the GPE (1.4) with a chemical potential μ_e [13, 12], i.e., (μ_e,ϕ_e) satisfying

$$\mu_e\phi_e(\mathbf{x}) = -\frac{1}{2}\nabla^2\phi_e+V_d(\mathbf{x})\phi_e+\beta_d|\phi_e|^2\phi_e-\Omega L_z\phi_e, \qquad \|\phi_e\|^2=1. \tag{2.27}$$

If the initial data $\psi_0(\mathbf{x})$ in (1.5) is chosen as a stationary state with a shift in its center, one can construct an exact solution of the GPE (1.4) with an harmonic oscillator potential (1.6). This kind of analytical construction can be used, in particular, in the benchmark and validation of numerical algorithms for the GPE. In [27], a similar kind of solution was constructed for the GPE and a second order ODE system was derived for the dynamics of the center, but the results there were valid only for nonrotating BEC, i.e., $\Omega = 0$. Modifications must be made for the rotating BEC, i.e., $\Omega \neq 0$. Later, in [15], similar results were extended to the case of a general Hamiltonian but

without specifying the initial data for the ODE system. For the convenience of the reader, here we present a simple derivation of the dynamic laws for rotating BEC.

LEMMA 2.4. *If the initial data* $\psi_0(\mathbf{x})$ *in* (1.5) *is chosen as*

$$\psi_0(\mathbf{x}) = \phi_e(\mathbf{x} - \mathbf{x}_0), \qquad \mathbf{x} \in \mathbb{R}^d, \tag{2.28}$$

where $\mathbf{x}_0$ *is a given point in* $\mathbb{R}^d$*, then the exact solution of* (1.4)–(1.5) *satisfies*

$$\psi(\mathbf{x}, t) = \phi_e(\mathbf{x} - \mathbf{x}(t))\, e^{-i\mu_e t}\, e^{iw(\mathbf{x},t)}, \quad \mathbf{x} \in \mathbb{R}^d, \quad t \geq 0, \tag{2.29}$$

where for any time $t \geq 0$*,* $w(\mathbf{x}, t)$ *is linear for* $\mathbf{x}$*, i.e.,*

$$w(\mathbf{x}, t) = \mathbf{c}(t) \cdot \mathbf{x} + g(t), \quad \mathbf{c}(t) = (c_1(t), \ldots, c_d(t))^T, \quad \mathbf{x} \in \mathbb{R}^d, \quad t \geq 0, \tag{2.30}$$

and $\mathbf{x}(t)$ *satisfies the following second-order ODE system:*

$$\ddot{x}(t) - 2\Omega\dot{y}(t) + \left(\gamma_x^2 - \Omega^2\right) x(t) = 0, \tag{2.31}$$

$$\ddot{y}(t) + 2\Omega\dot{x}(t) + \left(\gamma_y^2 - \Omega^2\right) y(t) = 0, \qquad t \geq 0, \tag{2.32}$$

$$x(0) = x_0, \quad y(0) = y_0, \quad \dot{x}(0) = \Omega y_0, \quad \dot{y}(0) = -\Omega x_0. \tag{2.33}$$

Moreover, if in $3D$*, another ODE needs to be added:*

$$\ddot{z}(t) + \gamma_z^2 z(t) = 0, \quad z(0) = z_0, \quad \dot{z}(0) = 0. \tag{2.34}$$

Proof. For $d = 2$, we introduce

$$J = \begin{pmatrix} 0 & 1 \\ -1 & 0 \end{pmatrix}, \quad A = \begin{pmatrix} \gamma_x^2 & 0 \\ 0 & \gamma_y^2 \end{pmatrix}, \quad \nabla = \begin{pmatrix} \partial_x \\ \partial_y \end{pmatrix}.$$

Differentiating (2.29) with respect to t and $\mathbf{x}$, respectively, plugging into (1.4), changing variable $\mathbf{x} - \mathbf{x}(t) \to \mathbf{x}$, and noticing (2.27), we obtain for $\phi_e = \phi_e(\mathbf{x})$ and $w = w(\mathbf{x} + \mathbf{x}(t), t)$ that

$$\begin{aligned} \phi_e \partial_t w + i\dot{\mathbf{x}}(t) \cdot \nabla\phi_e = \frac{1}{2}\left[i\phi_e \nabla^2 w - \phi_e |\nabla w|^2 - \mathbf{x}(t)^T A(2\mathbf{x} + \mathbf{x}(t))\phi_e\right] \\ + i\nabla\phi_e \cdot \nabla w - \phi_e \Omega(\mathbf{x} + \mathbf{x}(t)) \cdot (J\nabla w) + i\Omega\mathbf{x}(t) \cdot (J\nabla\phi_e). \end{aligned} \tag{2.35}$$

Taking the real and imaginary parts in (2.35) and noticing (2.30), we have

$$[\dot{\mathbf{x}}(t) - \nabla w(\mathbf{x} + \mathbf{x}(t), t) - \Omega J\mathbf{x}(t)] \cdot \nabla\phi_e = 0, \tag{2.36}$$

$$\left[\partial_t w + \frac{1}{2}|\nabla w|^2 + \frac{1}{2}\mathbf{x}(t)^T A(2\mathbf{x} + \mathbf{x}(t)) - \Omega(\mathbf{x} + \mathbf{x}(t)) \cdot (J\nabla w)\right] \phi_e = 0. \tag{2.37}$$

We thus get

$$\dot{\mathbf{x}}(t) = \nabla w(\mathbf{x} + \mathbf{x}(t), t) + \Omega J\mathbf{x}(t), \tag{2.38}$$

$$\begin{aligned} \partial_t w(\mathbf{x} + \mathbf{x}(t), t) = -\frac{1}{2}\left[|\nabla w|^2 + \mathbf{x}(t)^T A(2\mathbf{x} + \mathbf{x}(t))\right] \\ + \Omega(\mathbf{x} + \mathbf{x}(t)) \cdot (J\nabla w). \end{aligned} \tag{2.39}$$

Differentiating (2.38) and (2.39) with respect to t and $\mathbf{x}$, respectively, and noticing (2.30), which implies that $|\nabla w|^2$ is independent of $\mathbf{x}$, we obtain

$$\begin{aligned}
0 &= \ddot{\mathbf{x}}(t) - \partial_t(\nabla w(\mathbf{x}+\mathbf{x}(t),t)) - \Omega J\dot{\mathbf{x}}(t)\\
&= \ddot{\mathbf{x}}(t) - \nabla(\partial_t w(\mathbf{x}+\mathbf{x}(t),t)) - \dot{\mathbf{x}}(t)\,\nabla^2 w(\mathbf{x}+\mathbf{x}(t),t) - \Omega J\dot{\mathbf{x}}(t)\\
&= \ddot{\mathbf{x}}(t) - \nabla(\partial_t w(\mathbf{x}+\mathbf{x}(t),t)) - \Omega J\dot{\mathbf{x}}(t)\\
&= \ddot{\mathbf{x}}(t) + A\mathbf{x}(t) - \Omega J\,[\dot{\mathbf{x}}(t) - \Omega J\mathbf{x}(t)] - \Omega J\dot{\mathbf{x}}(t)\\
&= \ddot{\mathbf{x}}(t) - 2\Omega J\dot{\mathbf{x}}(t) + (A+\Omega^2 J^2)\mathbf{x}(t)\\
&= \ddot{\mathbf{x}}(t) - 2\Omega J\dot{\mathbf{x}}(t) + (A-\Omega^2 I)\mathbf{x}(t), \qquad t\ge 0. \qquad (2.40)
\end{aligned}$$

From (2.29) with $t=0$, we get

$$\mathbf{x}(0)=\mathbf{x}_0, \quad w(\mathbf{x},0)\equiv 0, \quad \mathbf{x}\in\mathbb{R}^d. \qquad (2.41)$$

Thus (2.33) is a combination of (2.41) and (2.38) with $t=0$. For $d=3$, the proof is similar, and the details are omitted here. □

In the literature, constructions similar to the above are often numerically verified by directly simulating the dynamics of the GPE in nonrotating BEC [14, 27]. To our knowledge, the above lemma gives the first rigorous derivation for rotating BEC.

Notice that if $\mathbf{u}=\dot{\mathbf{x}}(t)-\Omega J\mathbf{x}(t)$, then (2.40) gives a coupled first-order system

$$\begin{cases} \dot{\mathbf{x}}(t) = \Omega J\mathbf{x}(t) + \mathbf{u},\\ \dot{\mathbf{u}}(t) = -A\mathbf{x}(t) + \Omega J\mathbf{u},\\ \mathbf{x}(0)=\mathbf{x}_0, \ \ \mathbf{u}(0)=0, \end{cases} \qquad (2.42)$$

which is a Hamiltonian system with the Hamiltonian $H(\mathbf{x},\mathbf{u}) = \Omega\mathbf{u}^T J\mathbf{x} + (\mathbf{u}^T\mathbf{u} + \mathbf{x}^T A\mathbf{x})/2$. The characteristic roots λ of the system are given by the equation

$$\lambda^4 + (\gamma_x^2+\gamma_y^2+2\Omega^2)\lambda^2 + (\gamma_x^2-\Omega^2)(\gamma_y^2-\Omega^2) = 0. \qquad (2.43)$$

The exact solutions of (2.42) may thus be completely determined.

We note not only that results on the dynamics of a stationary state with its center shifted are physically interesting this type of exact solution of the time-dependent GPE can also serve as a good benchmark for numerical algorithms and is useful in the mathematical studies of the dynamic stabilities of the vortex state in BEC. In section 4.2, we will study this kind of dynamics by directly simulating the GPE in a rotational frame and explore different motion patterns of a stationary state center under different rotation speed Ω.

2.4. Dynamics of the total density in the presence of dissipation. Consider a more general GPE of the form

$$(i-\lambda)\partial_t\psi(\mathbf{x},t) = -\frac{1}{2}\nabla^2\psi + V(\mathbf{x},t)\psi + \beta_d|\psi|^2\psi - \Omega L_z\psi, \quad \mathbf{x}\in\mathbb{R}^d, \quad t>0, \qquad (2.44)$$

$$\psi(\mathbf{x},0)=\psi_0(\mathbf{x}), \quad \mathbf{x}\in\mathbb{R}^d, \qquad (2.45)$$

where $\lambda\ge 0$ is a real parameter that models a dissipation mechanism [2, 30, 32] and $V(\mathbf{x},t) = V_d(\mathbf{x}) + W(\mathbf{x},t)$ with $W(\mathbf{x},t)$ an external driven field [16, 31]. Typical external driven fields used in physics literature include a Delta kicked potential [31]

$$W(x,t) = K_s\cos(k_s x)\sum_{n=-\infty}^{\infty}\delta(t-n\tau), \qquad (2.46)$$

with K_s being the kick strength, k_s the wavenumber, τ the time interval between kicks, and $\delta(\tau)$ the Dirac delta function, or a far-blue detuned Gaussian laser beam stirrer [16]

$$W(\mathbf{x},t) = W_s(t)\exp\left[-\left(\frac{|\mathbf{x}-\mathbf{x}_s(t)|^2}{w_s/2}\right)\right] \tag{2.47}$$

with $W_s(t)$ being the height, w_s the width, and $\mathbf{x}_s(t)$ the position of the stirrer. In addition, we note that to study the onset of energy dissipation in BEC stirred by a laser field, another possibility is to view the beam as an translating *obstacle* [2] instead of introducing the Gaussian potential.

While the total density remains constant with $\lambda = 0$, in the more general case, we have the following lemma for the dynamics of the total density.

LEMMA 2.5. *Let $\psi(\mathbf{x},t)$ be the solution of (2.44)–(2.45); then the total density satisfies*

$$\dot{N}(\psi)(t) = \frac{d}{dt}\int_{\mathbb{R}^d}|\psi(\mathbf{x},t)|^2\,d\mathbf{x} = -\frac{2\lambda}{1+\lambda^2}\mu_{\beta,\Omega}(\psi), \qquad t\geq 0, \tag{2.48}$$

where

$$\mu_{\beta,\Omega}(\psi) = \int_{\mathbb{R}^d}\left[\frac{1}{2}|\nabla\psi|^2 + V(\mathbf{x},t)|\psi|^2 + \beta_d|\psi|^4 - \Omega\mathrm{Re}(\psi^* L_z\psi)\right]d\mathbf{x}.$$

Consequently, the total density decreases when $\lambda > 0$ and $|\Omega| \leq \gamma_{xy} := \min\{\gamma_x,\gamma_y\}$.

Proof. Dividing (2.44) by $(i-\lambda)$, multiplying it by ψ^* and summing with its complex conjugate, and integrating by parts, we obtain

$$\begin{aligned}
\frac{dN(\psi)}{dt} &= \int_{\mathbb{R}^d}\Bigg[-\frac{i+\lambda}{1+\lambda^2}\left(-\frac{1}{2}\nabla^2\psi + V(\mathbf{x},t)\psi + \beta_d|\psi|^2\psi - \Omega L_z\psi\right)\psi^* \\
&\qquad + \frac{i-\lambda}{1+\lambda^2}\left(-\frac{1}{2}\nabla^2\psi^* + V(\mathbf{x},t)\psi^* + \beta_d|\psi|^2\psi^* - \Omega(L_z)^*\psi^*\right)\psi\Bigg]d\mathbf{x} \\
&= \frac{\lambda}{1+\lambda^2}\int_{\mathbb{R}^d}\Bigg[\frac{1}{2}\left(\psi^*\nabla^2\psi + \psi\nabla^2\psi^*\right) - 2\left(V(\mathbf{x},t)|\psi|^2 + \beta_d|\psi|^4\right) \\
&\qquad\qquad + \Omega\left(\psi^* L_z\psi + \psi(L_z)^*\psi^*\right)\Bigg]d\mathbf{x} \\
&= \frac{-2\lambda}{1+\lambda^2}\int_{\mathbb{R}^d}\left[\frac{1}{2}|\nabla\psi|^2 + V(\mathbf{x},t)|\psi|^2 + \beta_d|\psi|^4 - \Omega\mathrm{Re}(\psi^* L_z\psi)\right]d\mathbf{x} \\
&= \frac{-2\lambda}{1+\lambda^2}\mu_{\beta,\Omega}(\psi). \qquad (2.49)
\end{aligned}$$

When $\gamma > 0$ and $|\Omega| < \gamma_{xy}$, by a completion of square [1, 13], we have

$$\frac{1}{2}|\nabla\psi|^2 + V(\mathbf{x},t)|\psi|^2 - \Omega\mathrm{Re}(\psi^* L_z\psi) = \frac{1}{2}|(\nabla - i\mathbf{A})\psi|^2 + \left[V(\mathbf{x},t) - \frac{|\Omega|^2}{2}(x^2+y^2)\right]|\psi|^2$$

for a vector potential $\mathbf{A} = \mathbf{A}(x,y) = (y,-x)\Omega$ in 2D and $\mathbf{A} = \mathbf{A}(x,y,z) = (y,-x,0)\Omega$ in 3D. Thus, $\mu_{\beta,\Omega}(\psi) > 0$. Consequently, we get

$$\frac{dN(\psi)}{dt} < 0, \qquad t\geq 0, \tag{2.50}$$

which immediately implies the decreasing of the total density. ∎

3. Numerical methods. In this section, we will present an efficient and accurate numerical method to solve the following GPE for the dynamics of rotating BEC.

Due to the trapping potential $V_d(\mathbf{x})$ given by (1.6), the solution $\psi(\mathbf{x},t)$ of (2.44)–(2.45) decays to zero exponentially fast when $|\mathbf{x}| \to \infty$. Thus in practical computation, we truncate the problem (2.44)–(2.45) into a bounded computational domain with the homogeneous Dirichlet boundary condition:

$$(i-\lambda)\partial_t\psi(\mathbf{x},t) = -\frac{1}{2}\nabla^2\psi + V(\mathbf{x},t)\psi + \beta_d|\psi|^2\psi - \Omega L_z\psi, \quad \mathbf{x}\in\Omega_{\mathbf{x}}, \quad t>0, \tag{3.1}$$

$$\psi(\mathbf{x},t) = 0, \quad \mathbf{x}\in\Gamma = \partial\Omega_{\mathbf{x}}, \quad t\geq 0, \tag{3.2}$$

$$\psi(\mathbf{x},0) = \psi_0(\mathbf{x}), \qquad \mathbf{x}\in\bar{\Omega}_{\mathbf{x}}, \tag{3.3}$$

where we choose $\Omega_{\mathbf{x}} = \{(x,y),\ r=\sqrt{x^2+y^2} < R\}$ in 2D and, respectively, $\Omega_{\mathbf{x}} = \{(x,y,z),\ r=\sqrt{x^2+y^2}<R,\ a<z<b\}$ in 3D with R, $|a|$, and b sufficiently large. The use of more sophisticated radiation boundary conditions is an interesting topic that remains to be examined in the future.

3.1. Time-splitting. We choose a time step size $\Delta t>0$. For $n=0,1,2,\ldots,$ from time $t=t_n=n\Delta t$ to $t=t_{n+1}=t_n+\Delta t$, the GPE (3.1) is solved in two splitting steps. One first solves

$$(i-\lambda)\ \partial_t\psi(\mathbf{x},t) = -\frac{1}{2}\nabla^2\psi - \Omega L_z\psi \tag{3.4}$$

for the time step of length Δt, followed by solving

$$(i-\lambda)\ \partial_t\psi(\mathbf{x},t) = V(\mathbf{x},t)\psi + \beta_d|\psi|^2\psi \tag{3.5}$$

for the same time step. Equation (3.4) will be discretized in detail in the next two subsections. For $t\in[t_n,t_{n+1}]$, after dividing (3.5) by $(i-\lambda)$, multiplying it by ψ^*, and adding with its complex conjugate, we obtain the following ODE for $\rho(\mathbf{x},t) = |\psi(\mathbf{x},t)|^2$:

$$\partial_t\rho(\mathbf{x},t) = -\frac{2\lambda}{1+\lambda^2}\left[V(\mathbf{x},t)\rho(\mathbf{x},t) + \beta_d\rho^2(\mathbf{x},t)\right], \quad \mathbf{x}\in\Omega_{\mathbf{x}}, \quad t_n\leq t\leq t_{n+1}. \tag{3.6}$$

The ODE for the phase angle $\phi(\mathbf{x},t)$ (determined as $\psi=\sqrt{\rho}e^{i\phi}$) is given by

$$\phi_t = -\frac{1}{1+\lambda^2}\left[V(\mathbf{x},t) + \beta_d\rho(\mathbf{x},t)\right], \quad \mathbf{x}\in\Omega_{\mathbf{x}}, \quad t_n\leq t\leq t_{n+1}. \tag{3.7}$$

For $\lambda\neq 0$, by (3.6), the above is equivalent to

$$\phi_t = \frac{1}{2\lambda}\partial_t\ln\rho, \quad \mathbf{x}\in\Omega_{\mathbf{x}}, \quad t_n\leq t\leq t_{n+1}. \tag{3.8}$$

Denoting $V_n(\mathbf{x},t) = \int_{t_n}^t V(\mathbf{x},\tau)d\tau$, we can solve (3.6) to get

$$\rho(\mathbf{x},t) = \frac{\rho(\mathbf{x},t_n)\ \exp[\frac{-2\lambda V_n(\mathbf{x},t)}{1+\lambda^2}]}{1+\rho(\mathbf{x},t_n)\frac{2\lambda\beta_d}{1+\lambda^2}\int_{t_n}^t \exp[\frac{-2\lambda V_n(\mathbf{x},\tau)}{1+\lambda^2}]\ d\tau}. \tag{3.9}$$

Consequently, in the special case $V(\mathbf{x},t) = V(\mathbf{x})$, we have some exact analytical solutions given by

$$\rho(\mathbf{x},t) = \begin{cases} \rho(\mathbf{x},t_n), & \lambda = 0, \\ \dfrac{(1+\lambda^2)\rho(\mathbf{x},t_n)}{(1+\lambda^2)+2\lambda\beta_d(t-t_n)\rho(\mathbf{x},t_n)}, & V(\mathbf{x}) = 0, \\ \dfrac{V(\mathbf{x})\rho(\mathbf{x},t_n)\ \exp[\frac{-2\lambda V(\mathbf{x})(t-t_n)}{1+\lambda^2}]}{V(\mathbf{x})+\left(1-\exp[\frac{-2\lambda V(\mathbf{x})(t-t_n)}{1+\lambda^2}]\right)\beta_d\rho(\mathbf{x},t_n)}, & V(\mathbf{x}) \neq 0. \end{cases} \tag{3.10}$$

Plugging (3.9) into (3.5), we get, for $t \in [t_n, t_{n+1}]$,

$$\psi(\mathbf{x},t) = \psi(\mathbf{x},t_n)\sqrt{U_n(\mathbf{x},t)}\exp\left[-\frac{i}{1+\lambda^2}\left(V_n(\mathbf{x},t)+\beta_d\int_{t_n}^{t}\rho(\mathbf{x},\tau)d\tau\right)\right], \tag{3.11}$$

where

$$U_n(\mathbf{x},t) = \frac{\exp[\frac{-2\lambda V_n(\mathbf{x},t)}{1+\lambda^2}]}{1+|\psi(\mathbf{x},t_n)|^2\frac{2\lambda\beta_d}{1+\lambda^2}\int_{t_n}^{t}\exp[\frac{-2\lambda V_n(\mathbf{x},\tau)}{1+\lambda^2}]\,d\tau}. \tag{3.12}$$

Again, with $V(\mathbf{x},t) = V(\mathbf{x})$, we can integrate exactly to get

$$\psi(\mathbf{x},t) = \psi(\mathbf{x},t_n)\begin{cases} \exp\left[-i(\beta_d|\psi(\mathbf{x},t_n)|^2+V(\mathbf{x}))(t-t_n)\right], & \lambda = 0, \\ \sqrt{\hat{U}_n(\mathbf{x},t)}\exp[\frac{i}{2\lambda}\ln\hat{U}_n(\mathbf{x},t)], & \lambda \neq 0, \end{cases} \tag{3.13}$$

where

$$\hat{U}_n(\mathbf{x},t) = \begin{cases} \dfrac{1+\lambda^2}{1+\lambda^2+2\lambda\beta_d(t-t_n)|\psi(\mathbf{x},t_n)|^2}, & V(\mathbf{x}) = 0, \\ \dfrac{V(\mathbf{x})\exp[-\frac{2\lambda(t-t_n)V(\mathbf{x})}{1+\lambda^2}]}{V(\mathbf{x})+\left(1-\exp[-\frac{2\lambda(t-t_n)V(\mathbf{x})}{1+\lambda^2}]\right)\beta_d|\psi(\mathbf{x},t_n)|^2}, & V(\mathbf{x}) \neq 0. \end{cases}$$

Remark 3.1. If the function $V_n(\mathbf{x},t)$ as well as other integrals in (3.9), (3.11), and (3.12) cannot be evaluated analytically, numerical quadrature can be used, e.g.,

$$V_n(\mathbf{x},t_{n+1}) = \int_{t_n}^{t_{n+1}} V(\mathbf{x},\tau)\,d\tau \approx \frac{\Delta t}{6}\left[V(\mathbf{x},t_n)+4V(\mathbf{x},t_n+\Delta t/2)+V(\mathbf{x},t_{n+1})\right].$$

3.2. Discretization in 2D. To solve (3.4), we try to formulate the equation in a variable separable form. When $d = 2$, we use the polar coordinate (r,θ) and discretize in the θ-direction by a Fourier pseudospectral method, in the r-direction by a finite element method (FEM), and in time by a Crank–Nicolson (C–N) scheme. Assume that

$$\psi(r,\theta,t) = \sum_{l=-L/2}^{L/2-1}\widehat{\psi}_l(r,t)\ e^{il\theta}, \tag{3.14}$$

where L is an even positive integer and $\widehat{\psi}_l(r,t)$ is the Fourier coefficient for the lth mode. Plugging (3.14) into (3.4) and noticing the orthogonality of the Fourier functions, we obtain, for $-\frac{L}{2} \le l \le \frac{L}{2} - 1$ and $0 < r < R$,

$$(i-\lambda)\,\partial_t \widehat{\psi}_l(r,t) = -\frac{1}{2r}\frac{\partial}{\partial r}\left(r\frac{\partial \widehat{\psi}_l(r,t)}{\partial r}\right) + \left(\frac{l^2}{2r^2} - l\Omega\right)\widehat{\psi}_l(r,t), \tag{3.15}$$

$$\widehat{\psi}_l(R,t) = 0 \quad (\text{for all } l), \qquad \widehat{\psi}_l(0,t) = 0 \quad (\text{for } l \neq 0). \tag{3.16}$$

Let P^k denote all polynomials with degree at most k, let $M > 0$ be a chosen integer, and $0 = r_0 < r_1 < r_2 < \cdots < r_M = R$ be a partition for the interval $[0, R]$ with a mesh size $h = \max_{0\le m<M}\{r_{m+1} - r_m\}$. Define a FEM subspace by

$$U^h = \left\{u^h \in C[0,R] \mid \ u^h\big|_{[r_m, r_{m+1}]} \in P^k,\ 0 \le m < M,\ u^h(R) = 0\right\}$$

for $l = 0$, and for $l \neq 0$,

$$U^h = \left\{u^h \in C[0,R] \mid \ u^h\big|_{[r_m, r_{m+1}]} \in P^k,\ 0 \le m < M,\ u^h(0) = u^h(R) = 0\right\};$$

then we obtain the FEM approximation for (3.15)–(3.16): Find $\hat{\psi}_l^h = \hat{\psi}_l^h(\cdot,t) \in U^h$ such that for all $\phi^h \in U^h$ and $t_n \le t \le t_{n+1}$,

$$(i-\lambda)\frac{d}{dt}A(\hat{\psi}_l^h(\cdot,t),\phi^h) = B(\hat{\psi}_l^h(\cdot,t),\phi^h) + l^2 C(\hat{\psi}_l^h,\phi^h) - l\Omega A(\hat{\psi}_l^h,\phi^h), \tag{3.17}$$

where

$$A(u^h,v^h) = \int_0^R r\ u^h(r)\ v^h(r)\ dr, \qquad B(u^h,v^h) = \int_0^R \frac{r}{2}\ \frac{du^h(r)}{dr}\ \frac{dv^h(r)}{dr}\ dr,$$
$$C(u^h,v^h) = \int_0^R \frac{1}{2r}\ u^h(r)\ v^h(r)\ dr, \qquad u^h,\ v^h \in U^h.$$

The ODE system (3.17) is then discretized by the standard C–N scheme in time. Although an implicit time discretization is applied for (3.17), the one-dimensional nature of the problem makes the coefficient matrix for the linear system band-limited. For example, if the piecewise linear polynomial is used, i.e., $k = 1$ in U^h, the matrix is tridiagonal. Fast algorithms can be applied to solve the resulting linear systems.

In practice, we always use the second-order Strang splitting [49]; i.e., from time $t = t_n$ to $t = t_{n+1}$ (i) evolve (3.5) for half time step $\Delta t/2$ with initial data given at $t = t_n$; (ii) evolve (3.4) for one time step Δt starting with the new data; (iii) evolve (3.5) for half time step $\Delta t/2$ with the newer data. For more general discussion on splitting methods, we refer the reader to [28, 38] for more details.

For the discretization considered here, the total memory requirement is $O(ML)$ and the total computational cost per time step is $O(ML \ln L)$. Furthermore, following the similar proofs in [6, 7, 14], the total density can be shown to be conserved in the discretized level when $\lambda = 0$ and to be decreased in the discretized level when $\lambda > 0$.

Remark 3.2. As noticed in [35, 34], another way for discretizing (3.15)–(3.16) is to use the finite difference in space on a mesh with a shifted grid and the C–N scheme in time. Choose an integer $M > 0$, a mesh size $\Delta r = 2R/(2M+1)$, and grid points

$r_m = (m-1/2)\Delta r$ for $0 \le m \le M+1$. Let $\hat{\psi}_{l,m}(t)$ be the approximation of $\hat{\psi}_l(r_m,t)$. A second-order finite difference discretization for (3.15)–(3.16) in space is

$$(i-\lambda)\frac{d\hat{\psi}_{l,m}(t)}{dt} = -\frac{r_{m+1/2}\hat{\psi}_{l,m+1}(t) - 2r_m\hat{\psi}_{l,m}(t) + r_{m-1/2}\hat{\psi}_{l,m-1}(t)}{2(\Delta r)^2 r_m} + \left(\frac{l^2}{2r_m^2} - l\Omega\right)\hat{\psi}_{l,m}(t), \quad m = 1,2,\ldots,M, \quad t_n \le t \le t_{n+1}, \tag{3.18}$$

with essential boundary conditions:

$$\hat{\psi}_{l,0}(t) = (-1)^l\hat{\psi}_{l,1}(t), \quad \hat{\psi}_{l,M+1}(t) = 0, \quad t_n \le t \le t_{n+1}. \tag{3.19}$$

The ODE system (3.18)–(3.19) may then be discretized in time by the C–N scheme so that only a tridiagonal linear system is to be solved with $O(M)$ arithmetic operations. We may further obtain a fourth-order finite difference discretization [35] for (3.15)–(3.16) on the interval $t \in [t_n, t_{n+1}]$:

$$\begin{aligned}(i-\lambda)\frac{d\hat{\psi}_{l,m}(t)}{dt} &= \left(\frac{l^2}{2r_m^2} - l\Omega\right)\hat{\psi}_{l,m}(t) \\ &\quad - \frac{-\hat{\psi}_{l,m+2}(t) + 16\hat{\psi}_{l,m+1}(t) - 30\hat{\psi}_{l,m}(t) + 16\hat{\psi}_{l,m-1}(t) - \hat{\psi}_{l,m-2}(t)}{24(\Delta r)^2} \\ &\quad - \frac{-\hat{\psi}_{l,m+2}(t) + 8\hat{\psi}_{l,m+1}(t) - 8\hat{\psi}_{l,m-1}(t) + \hat{\psi}_{l,m-2}(t)}{24\Delta r\ r_m}, \quad 1 \le m \le M, \end{aligned} \tag{3.20}$$

$$\begin{aligned}(i-\lambda)\frac{d\hat{\psi}_{l,M+1}(t)}{dt} &= \left(\frac{l^2}{2r_{M+1}^2} - l\Omega\right)\hat{\psi}_{l,M+1}(t) \\ &\quad - \frac{11\hat{\psi}_{l,M+2}(t) - 20\hat{\psi}_{l,M+1}(t) + 6\hat{\psi}_{l,M}(t) + 4\hat{\psi}_{l,M-1}(t) - \hat{\psi}_{l,M-2}(t)}{24(\Delta r)^2} \\ &\quad - \frac{3\hat{\psi}_{l,M+2}(t) + 10\hat{\psi}_{l,M+1}(t) - 18\hat{\psi}_{l,M}(t) + 6\hat{\psi}_{l,M-1}(t) - \hat{\psi}_{l,M-2}(t)}{24\Delta r\ r_{M+1}}, \end{aligned} \tag{3.21}$$

$$\hat{\psi}_{l,-1}(t) = (-1)^l\hat{\psi}_{l,2}(t), \quad \hat{\psi}_{l,0}(t) = (-1)^l\hat{\psi}_{l,1}(t), \quad \hat{\psi}_{l,M+1}(t) = 0. \tag{3.22}$$

Again the ODE system (3.20)–(3.22) may be discretized in time by the C–N scheme, and only a pentadiagonal linear system is to be solved, which can be done very efficiently too, i.e., via $O(M)$ arithmetic operations.

3.3. Discretization in 3D. When $d = 3$ in (3.4), we use the cylindrical coordinate (r,θ,z) and discretize in the θ-direction by the Fourier pseudospectral method, in the z-direction by the sine pseudospectral method, and in the r-direction by the finite element or finite difference method and in time by the C–N scheme. Assume that

$$\psi(r,\theta,z,t) = \sum_{l=-L/2}^{L/2-1}\sum_{k=1}^{K-1}\widehat{\psi}_{l,k}(r,t)\ e^{il\theta}\ \sin(\mu_k(z-a)), \tag{3.23}$$

where L and K are two even positive integers, $\mu_k = \frac{\pi k}{b-a}$ $(k = 1,\ldots,K-1)$, and $\widehat{\psi}_{l,k}(r,t)$ is the Fourier-sine coefficient for the (l,k)th mode. Plugging (3.23) into

(3.4) with $d = 3$ and noticing the orthogonality of the Fourier-sine modes, we obtain, for $-\frac{L}{2} \le l \le \frac{L}{2} - 1$, $1 \le k \le K - 1$, and $0 < r < R$, that

$$(i - \lambda)\,\partial_t \widehat{\psi}_{l,k}(r,t) = -\frac{1}{2r}\frac{\partial}{\partial r}\left(r\frac{\partial \widehat{\psi}_{l,k}(r,t)}{\partial r}\right) + \left(\frac{l^2}{2r^2} + \frac{\mu_k^2}{2} - l\Omega\right)\widehat{\psi}_{l,k}(r,t) \tag{3.24}$$

with essential boundary conditions

$$\widehat{\psi}_{l,k}(R,t) = 0 \text{ (for all } l), \qquad \widehat{\psi}_{l,k}(0,t) = 0 \text{ (for } l \neq 0). \tag{3.25}$$

The discretization of (3.24)–(3.25) is similar as that for (3.15)–(3.16) and is omitted here.

For the algorithm in 3D, the total memory requirement is $O(MLK)$ and the total computational cost per time step is $O(MLK \ln(LK))$.

4. Numerical simulations. In this section, we first test the accuracy of our numerical method. Then we apply it to study the dynamics of condensate width, a central vortex state with a shift in its center, and a quantized vortex lattice. Properties such as the conservation of energy and the angular momentum expectation and the stability of central vortices in rotating BEC are also discussed.

4.1. Numerical accuracy. To test the accuracy of our method, we take $d = 2$, $\lambda = 0$, $\gamma_x = \gamma_y = 1$, $\Omega = 0.8$, and $W(\mathbf{x}, t) \equiv 0$ in (2.44). The initial condition in (2.45) is taken as

$$\psi_0(\mathbf{x}) = \frac{2^{1/4}}{\pi^{1/2}} e^{-(x^2+2y^2)/2}, \qquad \mathbf{x} \in \mathbb{R}^2.$$

We take $R = 12$ for the bounded computational domain $\Omega_{\mathbf{x}}$ and the piecewise linear polynomial for U^h. Let ψ be the *exact* solution which is obtained numerically using our method with a very fine mesh and small time step, e.g., $\Delta r = \frac{1}{1024}$, $\Delta\theta = \frac{\pi}{128}$, and $\Delta t = 0.0001$, and let $\psi^{(\Delta r, \Delta\theta, \Delta t)}$ be the numerical solution obtained with mesh size $(\Delta r, \Delta\theta)$ and time step Δt.

First, we test the spectral accuracy in the θ-direction by choosing a very small mesh size in the r-direction $\Delta r = \frac{1}{1024}$ and the time step $\Delta t = 0.0001$ and by solving the problem for each fixed β_2 with different mesh size $\Delta\theta$ so that the discretization errors in the r-direction and in time can be neglected comparing to that in the θ-direction. The errors $||\psi(t) - \psi^{(\Delta r, \Delta\theta, \Delta t)}(t)||_{l^2}$ at $t = 2.0$ are shown in Table 4.1 for different values of β_2 and $\Delta\theta$.

Then we test the second-order accuracy in the r-direction by choosing a very fine mesh size $\Delta\theta = \frac{\pi}{128}$ and time step $\Delta t = 0.0001$ and by solving the problem with different values of β_2 and Δr. Table 4.2 shows the errors at $t = 2.0$ for different values of β_2 and Δr.

TABLE 4.1
Discretization error $\|\psi(t) - \psi^{(\Delta r, \Delta\theta, \Delta t)}(t)\|_{l^2}$ *at* $t = 2.0$ *in the* θ*-direction.*

Mesh size $\Delta\theta$	$\pi/2$	$\pi/4$	$\pi/8$	$\pi/16$	$\pi/32$
$\beta_2 = 0$	9.448E-2	1.203E-2	5.059E-4	4.981E-7	6.987E-13
$\beta_2 = 10$	0.3351	1.868E-2	4.408E-4	3.078E-7	7.597E-13
$\beta_2 = 50$	0.8577	8.609E-2	2.221E-3	1.527E-6	1.059E-12
$\beta_2 = 100$	1.1345	0.1994	9.415E-3	1.008E-5	3.553E-11

TABLE 4.2
Discretization error $\|\psi(t) - \psi^{(\Delta r, \Delta\theta, \Delta t)}(t)\|_{l^2}$ *at* $t = 2.0$ *in the* r*-direction.*

Mesh size Δr	1/32	1/64	1/128	1/256	1/512
$\beta_2 = 0$	2.716E-4	6.771E-5	1.673E-5	3.983E-6	7.968E-7
$\beta_2 = 10$	6.349E-3	1.586E-3	3.921E-4	9.337E-5	1.868E-5
$\beta_2 = 50$	0.1118	2.959E-2	7.358E-3	1.753E-3	3.507E-4
$\beta_2 = 100$	0.5203	0.1840	4.734E-2	1.131E-2	2.263E-3

TABLE 4.3
Discretization error $\|\psi(t) - \psi^{(\Delta r, \Delta\theta, \Delta t)}(t)\|_{l^2}$ *at* $t = 2.0$ *in time.*

Time step Δt	1/160	1/320	1/640	1/1280	1/2560
$\beta_2 = 0$	7.812E-5	1.952E-5	4.864E-6	1.201E-6	2.856E-7
$\beta_2 = 10$	2.236E-3	5.582E-4	1.391E-4	3.433E-5	8.155E-6
$\beta_2 = 50$	0.1111	3.581E-2	9.394E-3	2.328E-3	5.531E-4
$\beta_2 = 100$	0.5445	0.3044	0.1032	2.654E-2	6.319E-3

Next, we test the second-order accuracy in time. Table 4.3 lists the errors at $t = 2.0$ for different values of β_2 and time steps Δt with a very fine mesh in space, e.g., $\Delta r = \frac{1}{1024}$ and $\Delta\theta = \frac{\pi}{128}$.

From Tables 4.1–4.3, we can conclude that our method is of spectral-order accuracy in the θ-direction, second-order accuracy in time, and second-order accuracy in the r-direction when the piecewise linear FEM is used. Usually, for given parameter's setup and initial data, the bigger the β_2, the larger the errors. This implies that more grid points and a small time step should be used when β_2 is larger in order to get high accuracy. Furthermore, additional numerical experiments have been tested to verify the fourth-order accuracy in the r-direction when the continuous piecewise cubic element space is used. Such cubic elements are always used for the U^h in the following simulations.

4.2. Dynamics of a stationary state with a shifted center. To verify the analytical solution (2.29) and to study the dynamics of a stationary state with a shifted center through the direct simulation of the GPE for the rotating BEC, we take $d = 2$, $\lambda = 0$, $\gamma_x = \gamma_y = 1$, $\beta_2 = 100$, and $W(\mathbf{x}, t) \equiv 0$ in (2.44). The initial condition in (2.45) is taken as

$$\psi_0(\mathbf{x}) = \phi_e(\mathbf{x} - \mathbf{x}_0), \quad \phi_e(\mathbf{x}) = f(r)e^{i\theta}, \quad \mathbf{x} \in \mathbb{R}^2,$$

where $\phi_e(\mathbf{x})$ is a central vortex state with winding number $m = 1$ under the same parameter set; i.e., $f(r)$ is found numerically by the methods proposed in [5, 13]. This setup corresponds to a shift of the trap center from the origin to $-\mathbf{x}_0$. We take $\mathbf{x}_0 = (1, 1)^T$, $R = 12$ for $\Omega_{\mathbf{x}}$, mesh size $\Delta r = 0.004$, $\Delta\theta = \frac{\pi}{64}$, and time step $\Delta t = 0.0001$. The trajectory and position of the central vortex center with respect to time t are shown in Figure 1 for different rotation speed Ω. Notice that for the parameters chosen, the characteristic roots of (2.43) are given by $\pm(|\Omega| \pm 1)i$. When $\Omega = 0$ or $\Omega = \pm 1$, we get roots with higher multiplicities; otherwise, we have four distinct pure imaginary roots, and the periodicity of the orbits is thus implied for rational values of the frequency Ω. For $\Omega = 0$, (2.31)–(2.33) reduces to $\ddot{\mathbf{x}}(t) + \mathbf{x}(t) = 0$ with $\dot{\mathbf{x}}(0) = 0$. It is easy to see that the trajectory is a straight line. For $\Omega = \pm 1$, (2.31)–(2.33) reduces to $\ddot{\mathbf{x}}(t) \mp 2J\dot{\mathbf{x}}(t) = 0$, which leads to $\dot{\mathbf{x}}(t) = Q(\pm 2t)\dot{\mathbf{x}}(0)$ with $Q(2t)$ being a rotation of angle $\pm 2t$. The trajectory thus stays as a circle. In addition,

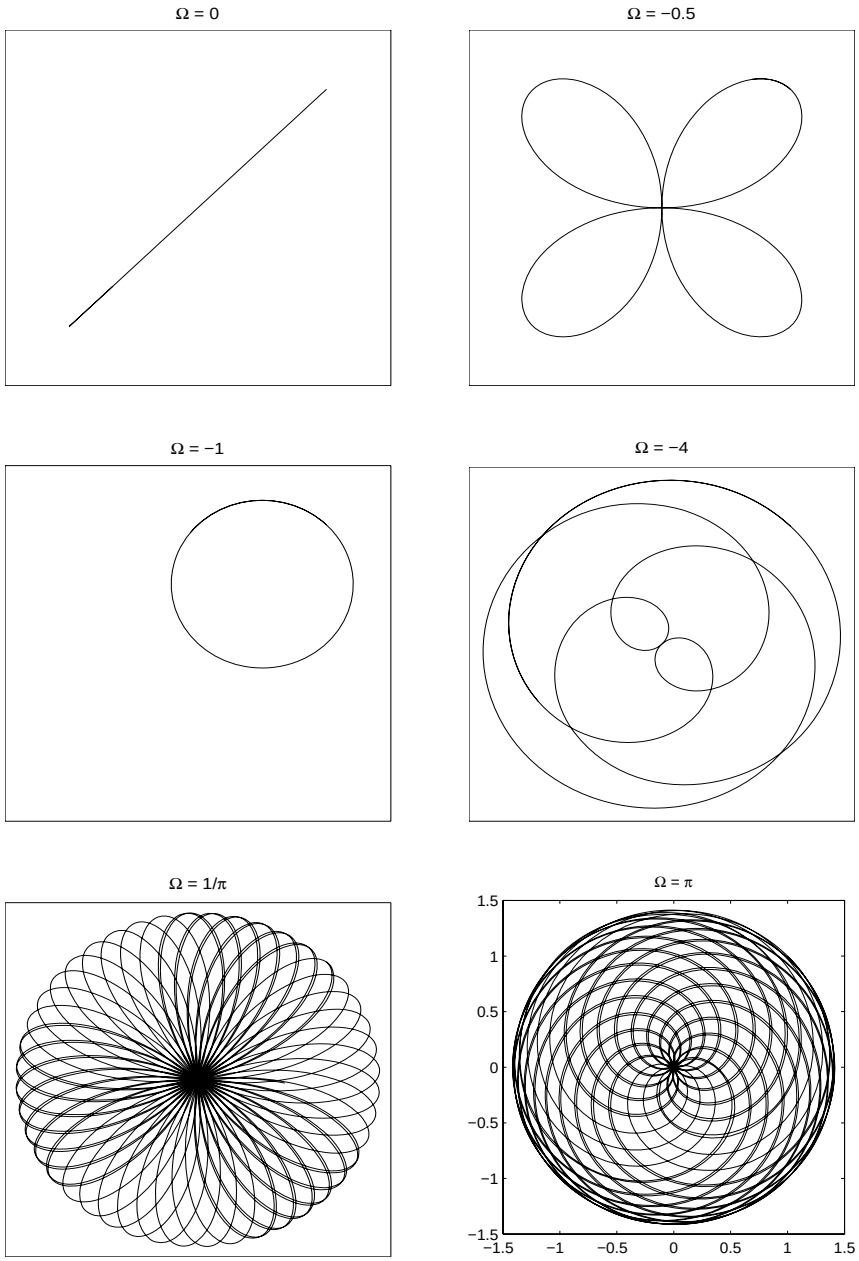

FIG. 1. *Trajectory of the central vortex center,* $\mathbf{x}(t) = (x(t), y(t))^T$ *for* $0 \le t \le 100$*, for different rotation speed* Ω*.*

for all other values of Ω, we can check that the equation is invariant under the rotation transformation, due to the fact that $Q(\theta)J = JQ(\theta)$ for any rotation matrix $Q(\theta)$. Thus, if $\Omega \neq 0, \pm 1$, and Ω is a rational number, there always exists a time t such that $e^{\pm i(\Omega \pm 1)t} = -1$; the trajectory thus always has the inversion symmetry (with respect to the origin). Other symmetries may also be explored for special values of Ω.

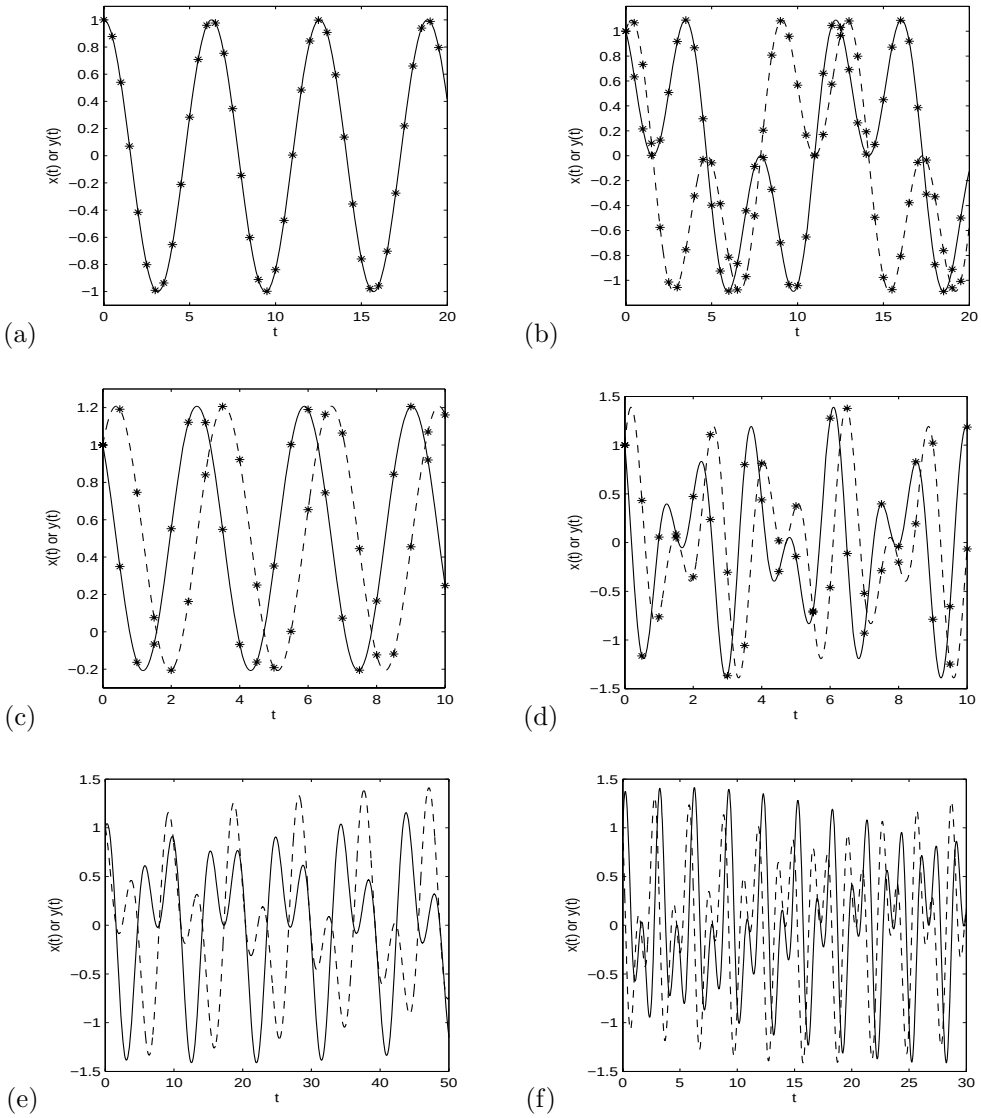

FIG. 1. (cont'd)*: Coordinates of the trajectory* $\mathbf{x}(t) = (x(t), y(t))^T$ *(solid line:* $x(t)$*; dashed line:* $y(t)$*).* (a): $\Omega = 0$*;* (b): $\Omega = -0.5$*;* (c): $\Omega = -1$*;* (d): $\Omega = -4$*;* (e): $\Omega = 1/\pi$*;* (f): $\Omega = \pi$*. In* (a)–(d)*, the solid and dashed lines are obtained from solving the GPE* (1.4)*, where "*" *is obtained from solving the ODE* (2.31)–(2.33)*.*

From Figure 1, we indeed see that when $\Omega = 0$, the center moves like a pendulum with period $T = 2\pi$; when $\Omega = -1$, it moves along a circle with period $T = \pi$. For other cases, the trajectory curve has inversion symmetry as predicted through the theoretical analysis. The solution trajectory and the coordinates in Figure 1 are obviously consistent with the above description of the solutions of the ODE system (2.31)–(2.33) for any given Ω. This provides a numerical verification of the exact solution constructed earlier for the GPE with an angular momentum rotation term and the reliability of our numerical scheme. Furthermore, based on Figure 1 and additional numerical experiments conducted, we find the following: (i) When Ω is a

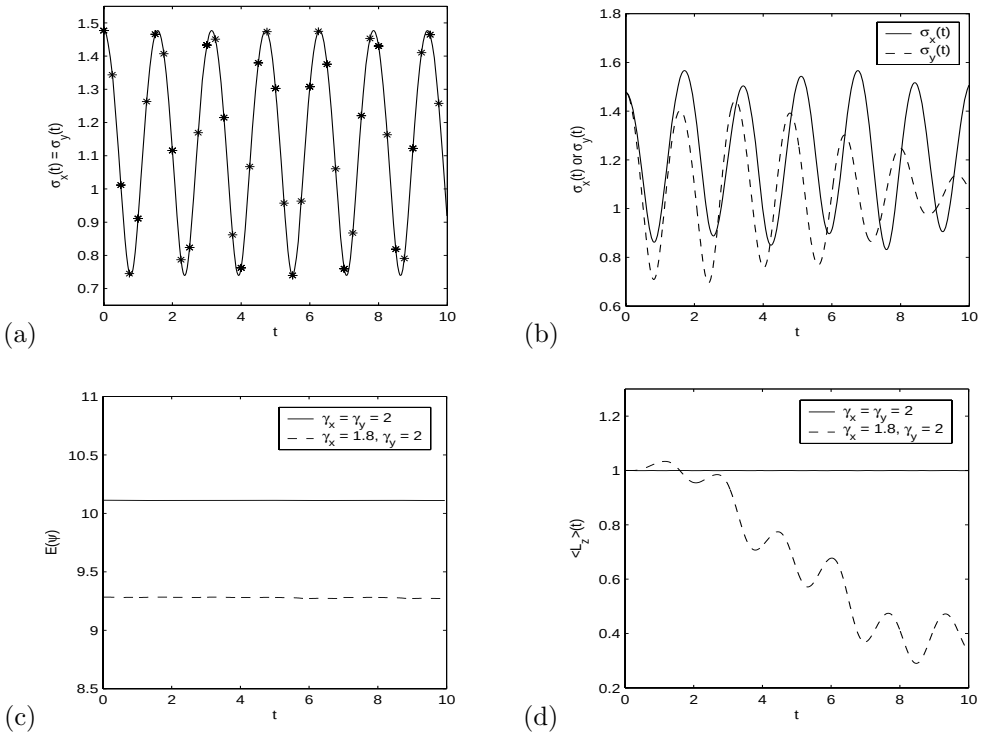

FIG. 2. *Time evolution of condensate widths (cf.* (a)*: $\gamma_x = \gamma_y = 2$; (b): $\gamma_x = 1.8$ and $\gamma_y = 2$), energy $E(\psi) := E_{\beta,\Omega}(\psi)$ (cf.* (c)*) and angular momentum expectation (cf.* (d)*). In* (a)*, the solid line is obtained from solving the GPE* (1.4) *and "*" is obtained from the analytical solution* (2.15).

rational number, i.e., $|\Omega| = q/p$ with q and p nonnegative integers and no common factor, then the trajectory of the vortex center moves periodically with period $p\pi$ if q and p are odd integers, and $2p\pi$ otherwise. (ii) When Ω is an irrational number, the trajectory of the vortex center moves chaotically, but the envelope of the trajectory is a circle centered at the origin with radius $r = |\mathbf{x}_0| = \sqrt{2}$ in our example (cf. Figure 1).

4.3. Dynamics of condensate width, energy, and angular momentum expectation. To verify the conservation of energy and angular momentum expectation as well as dynamics of condensate width, we take $d = 2$, $\lambda = 0$, $\beta_2 = 100$, $\Omega = 0.8$, and $W(\mathbf{x}, t) \equiv 0$ in (2.44). The initial condition in (2.45) is taken as the central vortex state with winding number $m = 1$ of the GPE with $\gamma_x = \gamma_y = 1$ [5, 14, 13], which is computed numerically by the method proposed in [5, 13]. Then at $t = 0$, we change the trap frequency by setting $\gamma_x = \gamma_y = 2$, or $\gamma_x = 1.8$ and $\gamma_y = 2$, respectively. Figure 2 shows the time evolution of condensate widths $\sigma_x(t)$ and $\sigma_y(t)$, the energy $E_{\beta,\Omega}(\psi)$, and the angular momentum expectation.

From Figure 2, we can see that (i) the condensate widths $\sigma_x(t)$ and $\sigma_y(t)$ are periodic functions of period $T = \pi/2$ when $\gamma_x = \gamma_y = 2$ (cf. Figure 2(a)) and periodic functions of period $T = \pi/2$ with a perturbation when $1.8 = \gamma_x \neq \gamma_y = 2$ (cf. Figure 2(b)), again confirming the analytical results (2.16) and (2.17), respectively; (ii) the energy $E_{\beta,\Omega}(\psi)$ is conserved in the discretized level (cf. Figure 2(c)); (iii) the angular momentum expectation is conserved when $\gamma_x = \gamma_y$ (cf. Figure 2(d) and the analytical result (2.3)). Furthermore, when $\gamma_x \neq \gamma_y$ and the initial condition is chosen as a

central vortex state with winding number $m = 1$, the angular momentum expectation is no longer conserved (cf. Figure 2(d)). We note that in the literature, there have been more studies both analytically and numerically on the thermodynamic stability of the central vortex state, though there is not much discussion available on the dynamic stability in real time. The experimental results shown here are thus of interest.

4.4. Dynamics of a quantized vortex lattice. Now we present the simulation results, via the algorithm discussed here, on the dynamics of a vortex lattice in rotating BEC under an anisotropic external perturber. We take $d = 2$, $\lambda = 0$, $\beta_2 = 1000$, $\gamma_x = \gamma_y = 1 := \gamma_r$, and $\Omega = 0.9$ in (2.44). The initial condition in (2.45) is taken as the ground state [13, 1] of the GPE with $W(\mathbf{x}, t) \equiv 0$, which is computed numerically by the normalized gradient flow with the backward Euler finite difference discretization proposed in [13]. For $t \geq 0$, an external perturber is introduced; i.e., $W(\mathbf{x}, t)$ in (2.44) is chosen as

$$W(\mathbf{x}, t) = \frac{\varepsilon}{2}\gamma_r^2 \left[(x^2 - y^2)\cos(2\tilde{\Omega}t) + 2xy\sin(2\tilde{\Omega}t)\right], \quad \mathbf{x} \in \mathbb{R}^2, \quad t \geq 0.$$

This implies the total potential $V(\mathbf{x}, t)$ in (2.44) is taken as

$$V(\mathbf{x}, t) = \frac{1}{2}\gamma_r^2 \left[(1+\epsilon)X(t)^2 + (1-\epsilon)Y(t)^2\right],$$

where $X(t) = x\cos(\tilde{\Omega}t) + y\sin(\tilde{\Omega}t)$, $Y(t) = y\cos(\tilde{\Omega}t) - x\sin(\tilde{\Omega}t)$.

This kind of time-dependent potential was used in [46] for studying the dynamics of nonrotating BEC. In our computation, we take $\epsilon = 0.35$, $\tilde{\Omega} = 0.75$, $R = 30$ for $\Omega_{\mathbf{x}}$, mesh size $\Delta r = 0.0075$ and $\Delta\theta = \frac{\pi}{128}$, and time step $\Delta t = 0.0001$. Figure 3 shows contour plots of the density function $|\psi(\mathbf{x}, t)|^2$ at different time steps.

For Figure 3, at $t = 0$, there are about 45 quantized vortices in the ground state. During the time evolution, the lattice is rotated due to the angular momentum term with different lattice patterns being formed due to the anisotropic external stirrer $W(\mathbf{x}, t)$. One may compare our numerical results with the experimental observations in [23], where the anisotropic compression of the vortex lattices was observed due to the dynamic distortion of the trap potentials.

4.5. Stability of central vortex states. Similarly as in [14, 16, 29, 30] for nonrotating BEC, we hereby also study numerically the stability of central vortex states in rotating BEC. We take $d = 2$, $\gamma_x = \gamma_y = 1$, $\beta_2 = 100$, $\Omega = -0.8$, and $\lambda = 0$ in (2.44). The initial condition in (2.45) is taken as a central vortex state [14, 5, 13] with winding number m of the GPE with $W(\mathbf{x}, t) \equiv 0$; i.e., $\psi_0(\mathbf{x}) = f_m(r)e^{im\theta}$, where $f_m(r)$ is computed numerically by the method proposed in [5, 14]. In order to study the stability, when $t \in [0, \pi/2]$, we introduce a far-blue detuned Gaussian laser beam stirrer (2.47), and when $t \geq \pi/2$, the perturber is removed. The parameters in (2.47) are chosen as

$$(x_s(t), y_s(t)) \equiv (3, 0), \quad \omega_s = 1, \quad W_s(t) = \begin{cases} 5\sin^2(2t), & t \in [0, \pi/2], \\ 0, & t \geq \pi/2. \end{cases}$$

In our computation, we take $R = 12$ for $\Omega_{\mathbf{x}}$, mesh size $\Delta r = 0.004$ and $\Delta\theta = \frac{\pi}{64}$, and time step $\Delta t = 0.0001$.

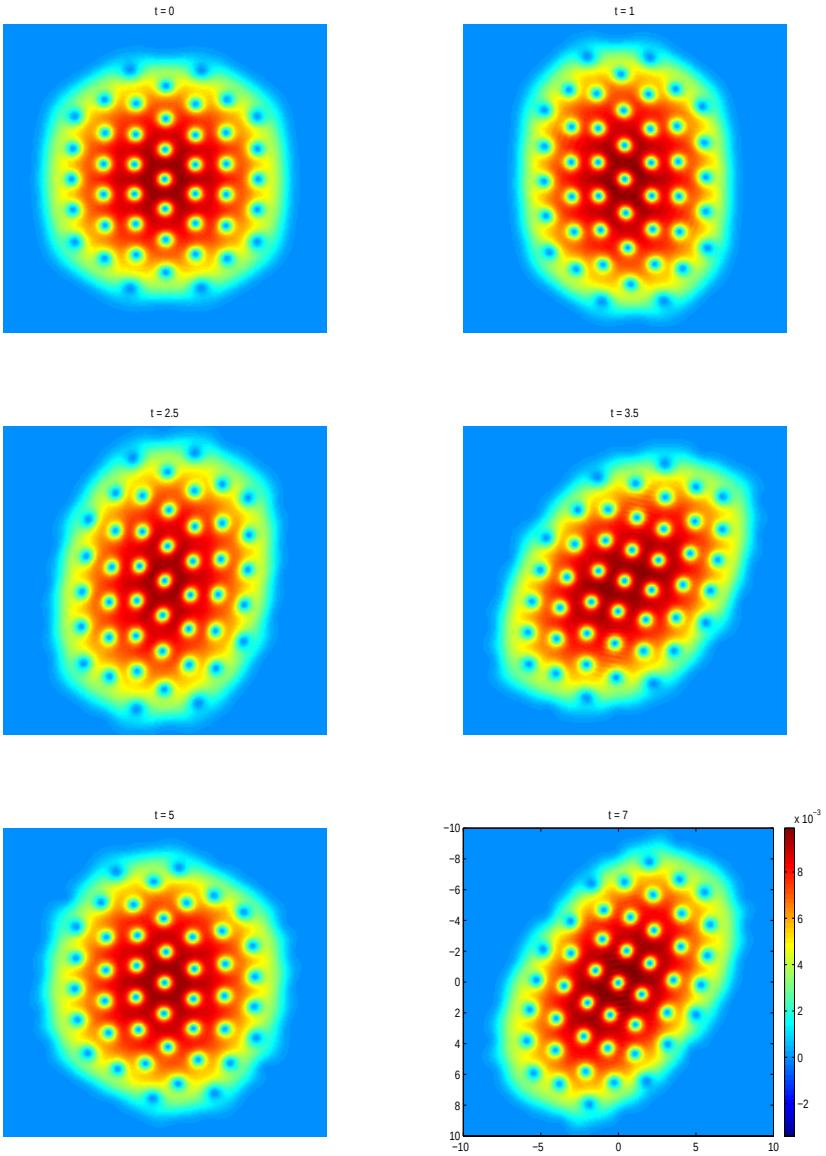

FIG. 3. *Contour plots of the density function* $|\psi(\mathbf{x}, t)|^2$ *for dynamics of a vortex lattice at different times.*

To quantitatively analyze the numerical results, we define the hydrodynamic velocity as

$$\mathbf{u} = (u, v) = \mathrm{Im}(\psi^* \nabla \psi)/|\psi|^2.$$

Figure 4 shows the velocity fields during the time evolution of the central vortex states with winding number $m = 1$ and $m = 2$, while the dynamic evolution of the energy and that of the angular momentum expectation are shown in Figure 5.

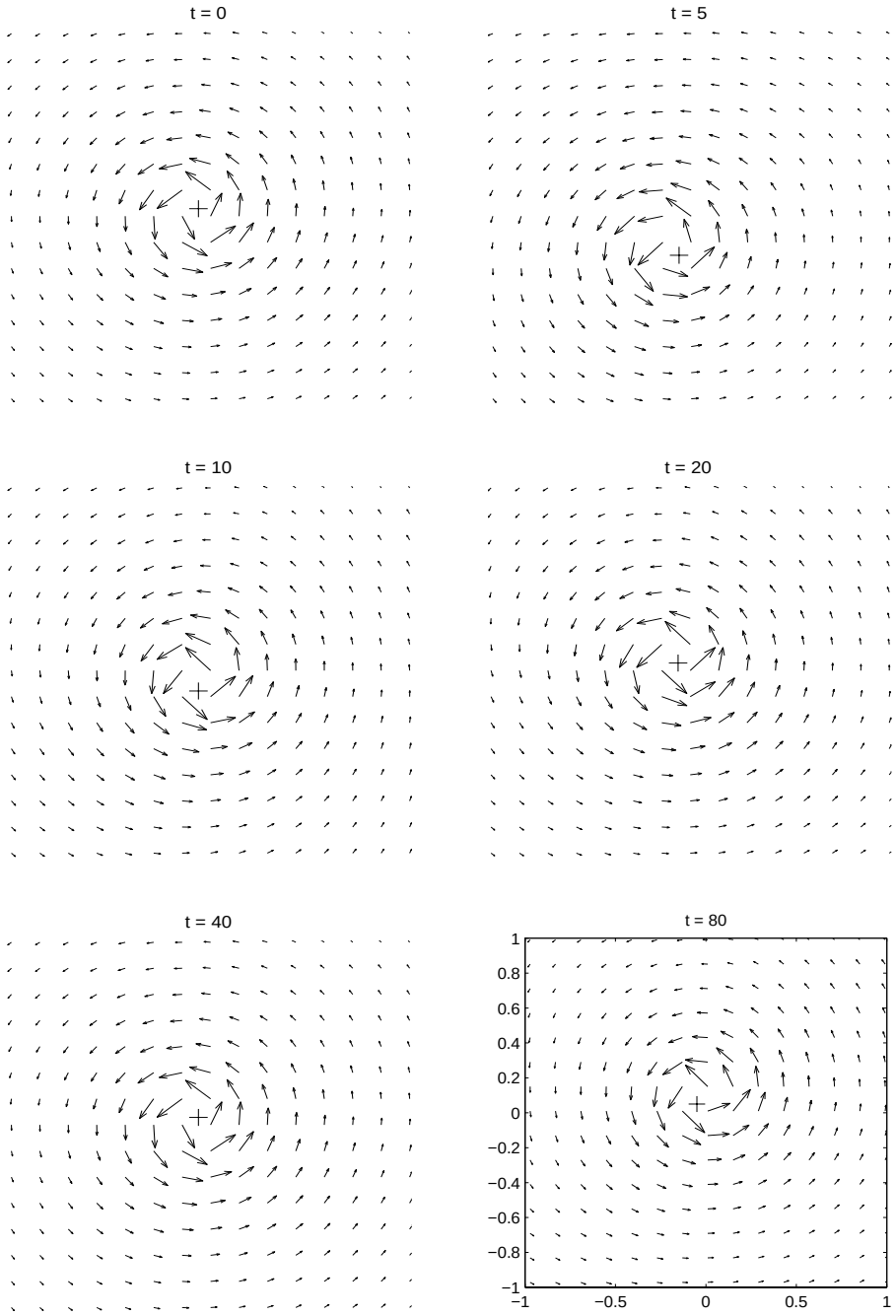

FIG. 4. *Velocity field at different times for stability of a central vortex state.* I. *For winding number* $m = 1$.

From Figure 4 and additional numerical experiments conducted, we find that the central vortex states with an index (or degree, winding number) $m = \pm 1$ are dynamically stable, but they are unstable when $|m| > 1$ in rotating BEC. Furthermore, Figure 5 depicts the increase in the energy and the decrease of the angular momentum

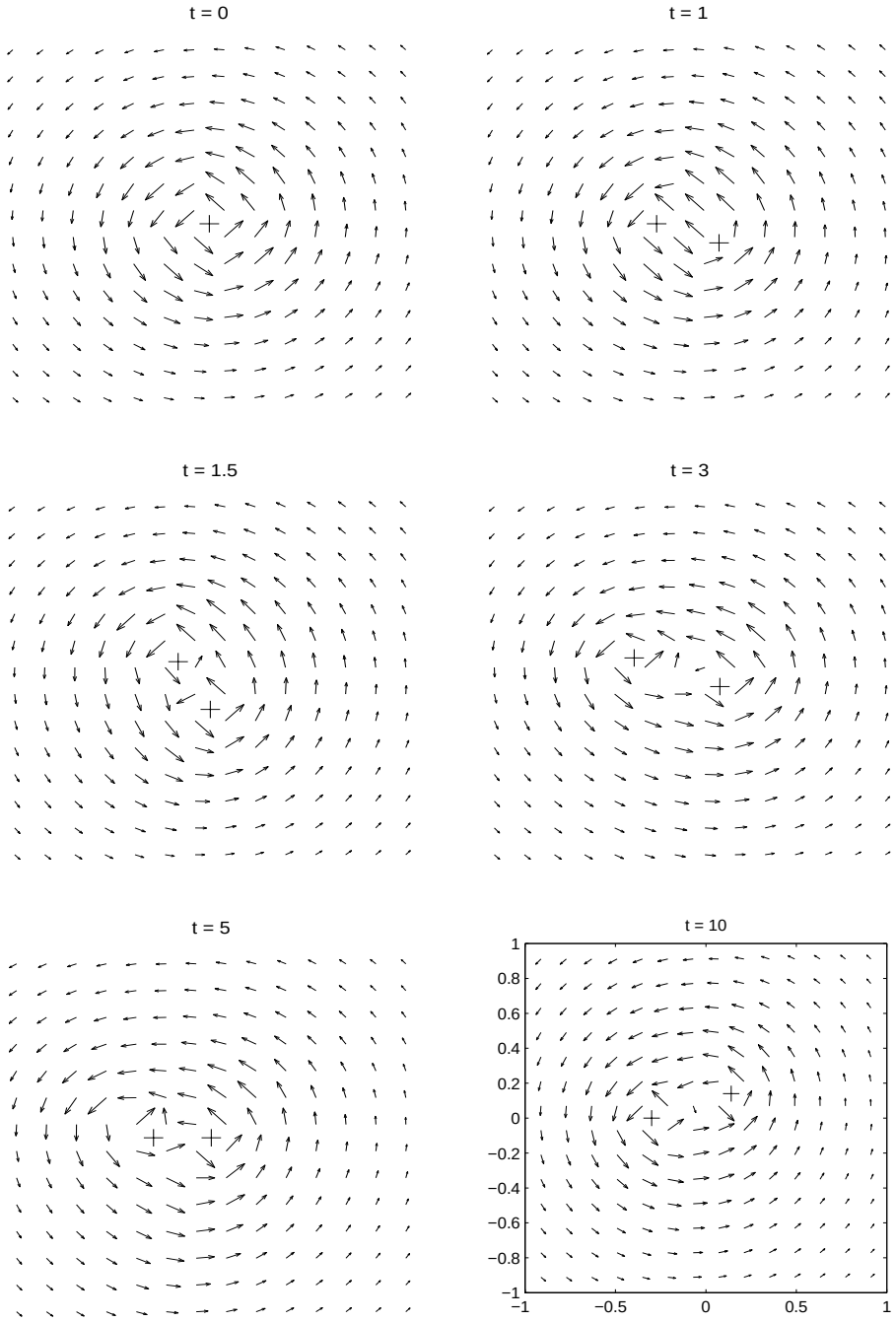

FIG. 4. (cont'd): II. *For* $m = 2$.

expectation when $t \in [0, \pi/2]$ due to the appearance of the perturber. After removing the perturber at $t = \pi/2$, they are conserved with time, which again confirm the conservation laws (1.8) and (2.3).

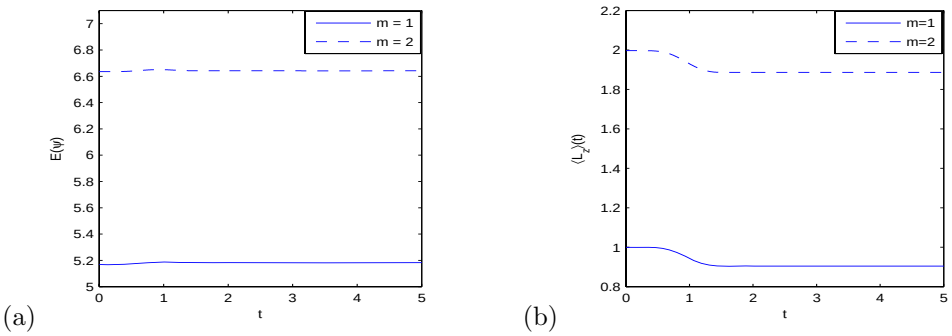

(a) (b)

FIG. 5. *Time evolution of energy* $E(\psi) := E_{\beta,\Omega}(\psi)$ *and angular momentum expectation* $\langle L_z \rangle$ *in studying the stability of central vortex states.*

4.6. Dissipation effect on the GPE. In order to study the effect of the damping mechanism in the GPE (2.44), we take $d = 2$, $\gamma_x = 1$, $\gamma_y = 1.1$, $\beta_2 = 500$, $\Omega = 0.9$, and $W(\mathbf{x}, t) \equiv 0$ in (2.44). The initial condition in (2.45) is taken as

$$\psi_0(\mathbf{x}) = \frac{(\gamma_x \gamma_y)^{1/4}}{\sqrt{\pi}} \, e^{-(\gamma_x x^2 + \gamma_y y^2)/2}, \qquad \mathbf{x} \in \mathbb{R}^2.$$

We take $R = 30$ for $\Omega_{\mathbf{x}}$, mesh size $\Delta r = 0.0075$ and $\Delta\theta = \frac{\pi}{64}$, and time step $\Delta t = 0.0001$. Figure 6 shows the normalized density $\frac{|\psi(\mathbf{x},t)|^2}{\|\psi(\cdot,t)\|^2}$ at different times for $\lambda = 0.03$, while Figure 7 illustrates the time evolution of the energy and angular momentum expectation per particle, i.e., $\frac{E_{\beta,\Omega}(\psi)}{\|\psi(\cdot,t)\|^2}$ and $\frac{\langle L_z \rangle}{\|\psi(\cdot,t)\|^2}$ for different $\lambda > 0$.

From Figures 6 and 7, we can see that when a dissipation term is applied to the GPE, a dent appears in the center of the density function during time evolution. The larger the damping parameter λ, the faster the energy per particle decreases and the slower the angular momentum expectation per particle increases. In fact, the change in the angular momentum expectation is due to the anisotropy of the external trapping potential, i.e., $\gamma_x \neq \gamma_y$.

5. Conclusion. We have studied the dynamics of the Gross–Pitaevskii equation with an angular momentum rotation term for rotating BEC both analytically and numerically. Along the analytical front, we proved the conservation of the angular momentum expectation when the external trapping potential is radially symmetric in 2D and, respectively, cylindrically symmetric in 3D. A second-order ODE was also derived to describe the time evolution of the condensate width as a periodic function with/without a perturbation, and the frequency of the periodic function doubles the trapping frequency. We also presented an ODE system with a complete initial data that governs the dynamics of a stationary state with a shifted center, and we also illustrated the decrease in the total density when a damping term is applied in the GPE. On the numerical side, we proposed an efficient, accurate, and unconditionally stable numerical method for simulating the rotating BEC with/without a time-dependent external perturber or a damping term. We also applied the new method to study numerically the dynamics of condensate including the condensate widths, energy, and angular momentum expectation as well as a quantized vortex lattice and a stationary state with a shifted center. We numerically found that, for the

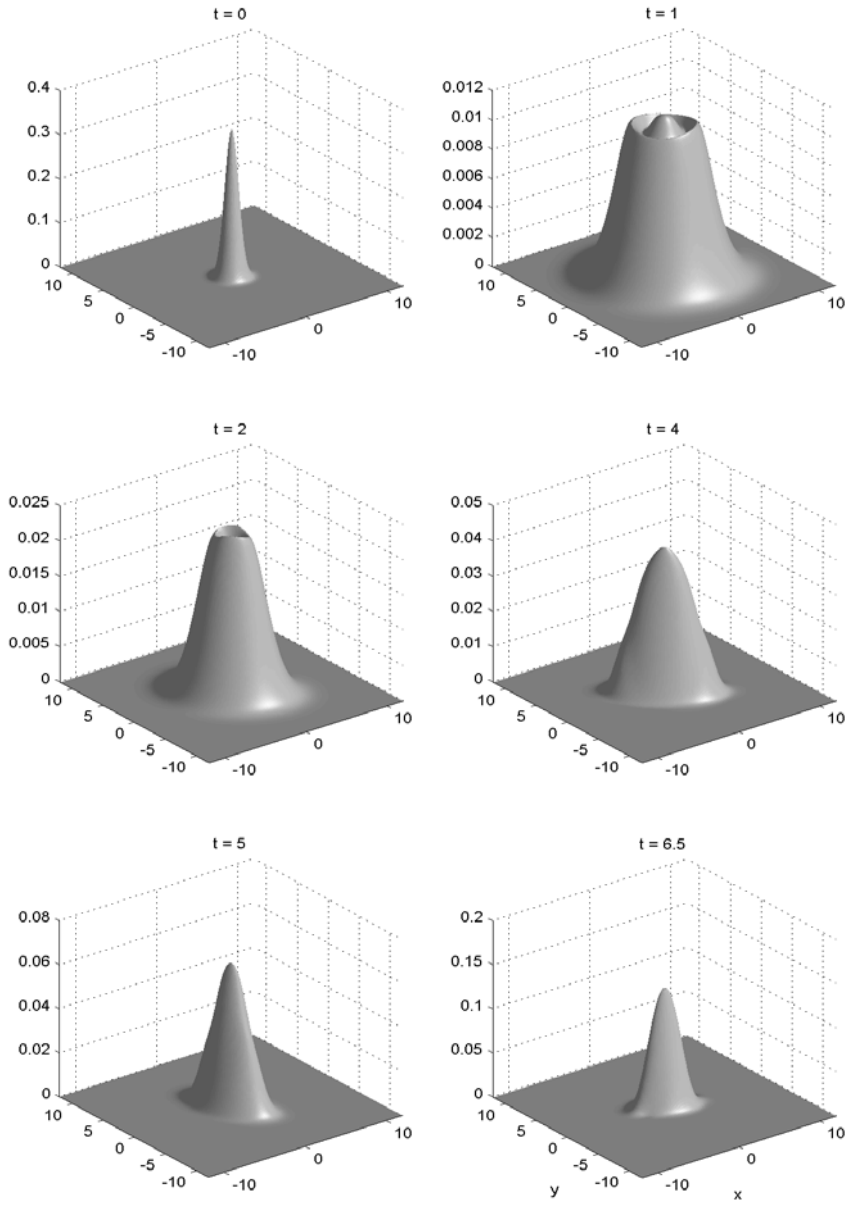

FIG. 6. *Surface plots of the normalized density function* $\frac{|\psi(\mathbf{x},t)|^2}{\|\psi(\cdot,t)\|^2}$ *in section* 4.6 *for GPE with a damping term at different times.*

real time dynamics, the central vortex states are dynamically stable only for the one with index (or winding number) $m = \pm 1$. In the future, this efficient and accurate numerical method can be used to study the dynamics and interaction of vortex line states in 3D for rotating BEC and to make more close comparisons with experimental findings [42, 47, 48].

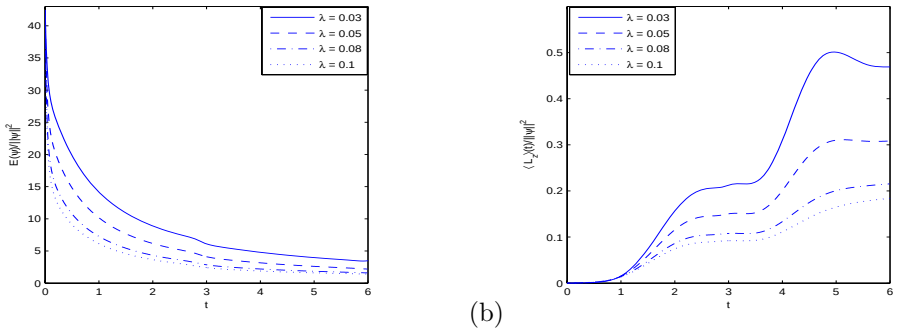

FIG. 7. *Time evolution of the energy per particle* $\frac{E_{\beta,\Omega}(\psi)}{\|\psi\|^2}$ *and angular momentum expectation* $\frac{\langle L_z\rangle}{\|\psi\|^2}$ *in section* 4.6 *for the GPE with a damping term.*

REFERENCES

[1] A. AFTALION AND Q. DU, *Vortices in a rotating Bose–Einstein condensate: Critical angular velocities and energy diagrams in the Thomas–Fermi regime*, Phys. Rev. A, 64 (2001), 063603.

[2] A. AFTALION, Q. DU, AND Y. POMEAU, *Dissipative flow and vortex shedding in the Painlevé boundary layer of a Bose–Einstein condensate*, Phy. Rev. Lett., 91 (2003), 090407.

[3] M. H. ANDERSON, J. R. ENSHER, M. R. MATTHEWA, C. E. WIEMAN, AND E. A. CORNELL, *Observation of Bose–Einstein condensation in a dilute atomic vapor*, Science, 269 (1995), pp. 198–201.

[4] W. BAO, *Ground states and dynamics of multicomponent Bose–Einstein condensates*, Multiscale Model. Simul., 2 (2004), pp. 210–236.

[5] W. BAO AND Q. DU, *Computing the ground state solution of Bose–Einstein condensates by a normalized gradient flow*, SIAM J. Sci. Comput., 25 (2004), pp. 1674–1697.

[6] W. BAO AND D. JAKSCH, *An explicit unconditionally stable numerical method for solving damped nonlinear Schrödinger equations with a focusing nonlinearity*, SIAM J. Numer. Anal., 41 (2003), pp. 1406–1426.

[7] W. BAO, D. JAKSCH, AND P. A. MARKOWICH, *Numerical solution of the Gross–Pitaevskii equation for Bose–Einstein condensation*, J. Comput. Phys., 187 (2003), pp. 318–342.

[8] W. BAO, D. JAKSCH, AND P. A. MARKOWICH, *Three dimensional simulation of jet formation in collapsing condensates*, J. Phys. B: At. Mol. Opt. Phys., 37 (2004), pp. 329–343.

[9] W. BAO, S. JIN, AND P. A. MARKOWICH, *On time-splitting spectral approximation for the Schrödinger equation in the semiclassical regime*, J. Comput. Phys., 175 (2002), pp. 487–524.

[10] W. BAO, S. JIN, AND P. A. MARKOWICH, *Numerical study of time-splitting spectral discretizations of nonlinear Schrödinger equations in the semiclassical regimes*, SIAM J. Sci. Comput., 25 (2003), pp. 27–64.

[11] W. BAO AND J. SHEN, *A fourth-order time-splitting Laguerre–Hermite pseudospectral method for Bose–Einstein condensates*, SIAM J. Sci. Comput., 26 (2005), pp. 2010–2028.

[12] W. BAO AND W. TANG, *Ground state solution of trapped interacting Bose–Einstein condensate by directly minimizing the energy functional*, J. Comput. Phys., 187 (2003), pp. 230–254.

[13] W. BAO, H. WANG, AND P. A. MARKOWICH, *Ground, symmetric and central vortex states in rotating Bose–Einstein condensates*, Commun. Math. Sci., 3 (2005), pp. 57–88.

[14] W. BAO AND Y. ZHANG, *Dynamics of the ground state and central vortex states in Bose–Einstein condensation*, Math. Models Methods Appl. Sci., 15 (2005), pp. 1863–1896.

[15] I. BIALYNICKI-BIRULA AND Z. BIALYNICKI-BIRULA, *Center-of-mass motion in the many-body theory of Bose–Einstein condensates*, Phys. Rev. A, 65 (2002), 063606.

[16] B. M. CARADOC-DAVIS, R. J. BALLAGH, AND K. BURNETT, *Coherent dynamics of vortex formation in trapped Bose–Einstein condensates*, Phys. Rev. Lett., 83 (1999), pp. 895–898.

[17] Y. CASTIN AND R. DUM, *Bose-Einstein condensates with vortices in rotating traps*, Eur. Phys. J. DAt. Mol. Opt. Phys., 7(1999), pp. 399–412.

[18] M. M. Cerimele, M. L. Chiofalo, F. Pistella, S. Succi, and M. P. Tosi, *Numerical solution of the Gross–Pitaevskii equation using an explicit finite-difference scheme: An application to trapped Bose–Einstein condensates*, Phys. Rev. E, 62 (2000), pp. 1382–1389.

[19] M. M. Cerimele, F. Pistella, and S. Succi, *Particle-inspired scheme for the Gross–Pitaevskii equation: An application to Bose–Einstein condensation*, Comput. Phys. Comm., 129 (2000), pp. 82–90.

[20] F. Dalfovo, S. Giorgini, L. P. Pitaevskii, and S. Stringari, *Theory of Bose–Einstein condensation in trapped gases*, Rev. Mod. Phys., 71 (1999), pp. 463–512.

[21] K. B. Davis, M. O. Mewes, M. R. Andrews, N. J. van Druten, D. S. Durfee, D. M. Kurn, and W. Ketterle, *Bose–Einstein condensation in a gas of sodium atoms*, Phys. Rev. Lett., 75 (1995), pp. 3969–3973.

[22] Q. Du, *Numerical computations of quantized vortices in Bose–Einstein condensate*, in Recent Progress in Computational and Applied PDEs, T. F. Chan, Y. Huang, T. Tang, J. Xu, and L.-A. Ying, eds., Kluwer Academic Publishers, Boston, Dordrecht, London, 2002, pp. 155–168.

[23] P. Engels, I. Coddington, P. Haijan, and E. Cornell, *Nonequilibrium effects of anisotropic compression applied to vortex lattices in Bose–Einstein condensates*, Phy. Rev. Lett, 89 (2002), 100403.

[24] D. L. Feder, C. W. Clark, and B. I. Schneider, *Nucleation of vortex arrays in rotating anisotropic Bose–Einstein condensates*, Phys. Rev. A, 61 (1999), 011601.

[25] D. L. Feder, C. W. Clark, and B. I. Schneider, *Vortex stability of interacting Bose–Einstein condensates confined in anisotropic harmonic traps*, Phys. Rev. Lett., 82 (1999), pp. 4956–4959.

[26] D. L. Feder, A. A. Svidzinsky, A. L. Fetter, and C. W. Clark, *Anomalous modes drive vortex dynamics in confined Bose–Einstein condensates*, Phys. Rev. Lett., 86 (2001), pp. 564–567.

[27] J. J. Garcia-Ripoll, V. M. Perez-Garcia, and V. Vekslerchik, *Construction of exact solutions by spatial translations in inhomogeneous nonlinear Schrödinger equations*, Phys. Rev. E, 64 (2001), 056602.

[28] R. Glowinski and P. Le Tallec, *Augmented Lagrangian and Operator Splitting Methods in Nonlinear Mechanics*, SIAM Stud. Appl. Math. 9, SIAM, Philadelphia, 1989.

[29] B. Jackson, J. F. McCann, and C. S. Adams, *Vortex formation in dilute inhomogeneous Bose–Einstein condensates*, Phys. Rev. Lett., 80 (1998), pp. 3903–3906.

[30] B. Jackson, J. F. McCann, and C. S. Adams, *Dissipation and vortex creation in Bose–Einstein condensate gases*, Phys. Rev. A, 61 (2000), 051603.

[31] D. Jaksch, C. Bruder, J. I. Cirac, C. W. Gardiner, and P. Zoller, *Cold bosonic atoms in optical lattices*, Phys. Rev. Lett., 81 (1998), pp. 3108–3111.

[32] A. M. Kamchatnov, A. Gammal, and R. A. Kraenkel, *Dissipationless shock waves in repulsive Bose–Einstein condensates*, Phys. Rev. A, 69 (2004), 063605.

[33] K. Kasamatsu, M. Tsubota, and M. Ueda, *Nonlinear dynamics of vortex lattice formation in a rotating Bose–Einstein condensate*, Phys. Rev. A, 67 (2003), 033610.

[34] M.-C. Lai, W.-W. Lin, and W. Wang, *A fast spectral/difference method without pole conditions for Poisson-type equations in cylindrical and spherical geometries*, IMA J. Numer. Anal., 22 (2002), pp. 537–548.

[35] M.-C. Lai and W.-C. Wang, *Fast direct solvers for Poisson equation on 2D polar and spherical geometries*, Numer. Methods Partial Differential Equations, 18 (2002), pp. 56–68.

[36] K. W. Madison, F. Chevy, W. Wohlleben, and J. Dalibard, *Vortex formation in a stirred Bose–Einstein condensate*, Phys. Rev. Lett., 84 (2000), pp. 806–809.

[37] K. W. Madison, F. Chevy, V. Bretin, and J. Dalibard, *Stationary states of a rotating Bose–Einstein condensate: Routes to vortex nucleation*, Phys. Rev. Lett., 86 (2001), pp. 4443–4446.

[38] G. Marchuk, *Splitting and alternating direction methods*, in Handbook of Numerical Analysis, North–Holland, Amsterdam, 1990.

[39] M. R. Matthews, B. P. Anderson, P. C. Haljan, D. S. Hall, C. E. Wiemann, and E. A. Cornell, *Vortices in a Bose–Einstein condensate*, Phys. Rev. Lett., 83 (1999), pp. 2498–2501.

[40] A. Minguzzi, S. Succi, F. Toschi, M. P. Tosi, and P. Vignolo, *Numerical methods for atomic quantum gases with applications to Bose–Einstein condensates and to ultracold fermions*, Phys. Rep., 395 (2004), pp. 223–355.

[41] P. Muruganandam and S. K. Adhikari, *Bose–Einstein condensation dynamics in three dimensions by pseudospectral and finite-difference methods*, J. Phys. B: At. Mol. Opt. Phys., 36 (2003), pp. 2501–2513.

[42] A. A. Penckwitt, R. J. Ballagh, and C. W. Gardiner, *Nucleation, growth, and stabilization of Bose–Einstein condensate vortex lattices*, Phys. Rev. Lett., 89 (2002), 260402.
[43] C. J. Pethick and H. Smith, *Bose–Einstein Condensation in Dilute Gases*, Cambridge University Press, Cambridge, UK, 2002.
[44] L. P. Pitaevskii and S. Stringari, *Bose–Einstein Condensation*, Clarendon Press, Oxford, UK, 2003.
[45] C. Raman, J. R. Abo-Shaeer, J. M. Vogels, K. Xu, and W. Ketterle, *Vortex nucleation in a stirred Bose–Einstein condensate*, Phys. Rev. Lett., 87 (2001), 210402.
[46] B. I. Schneider and D. L. Feder, *Numerical approach to the ground and excited states of a Bose–Einstein condensed gas confined in a completely anisotropic trap*, Phys. Rev. A, 59 (1999), pp. 2232–2242.
[47] T. P. Simula, P. Engels, I. Coddington, V. Schweikhard, E. A. Cornell, and R. J. Ballagh, *Observations on sound propagation in rapidly rotating Bose–Einstein condensates*, Phys. Rev. Lett., 94 (2005), 080404.
[48] T. P. Simula, A. A. Penckwitt, and R. J. Ballagh, *Giant vortex lattice deformations in rapidly rotating Bose–Einstein condensates*, Phys. Rev. Lett., 92 (2004), 060401.
[49] G. Strang, *On the construction and comparison of difference schemes*, SIAM J. Numer. Anal., 5 (1968), pp. 506–517.